miR-252 targeting temperature receptor *CcTRPM* to mediate the transition from summer-form to winter-form of *Cacopsylla chinensis*

Songdou Zhang, Jianying Li, Dongyue Zhang, Zhixian Zhang, Shili Meng, Zhen Li, Xiaoxia Liu*
Department of Entomology and MOA Key Lab of Pest Monitoring and Green Management, College of Plant Protection, China Agricultural University, 100193 Beijing, China
* Corresponding author. E-mail address: liuxiaoxia611@cau.edu.cn (Xiaoxia Liu).

Abstract:
Temperature determines the geographical distribution of organisms and affects the outbreak and damage of pests. Insects seasonal polyphenism is a successful strategy adopted by some species to adapt the changeable external environment. *Cacopsylla chinensis* (Yang & Li) showed two seasonal morphotypes, summer-form and winter-form, with significant differences in morphological characteristics. Low temperature is the key environmental factor to induce its transition from summer-form to winter-form. However, the detailed molecular mechanism remains unknown. Here, we firstly confirmed that low temperature of 10°C induced the transition from summer-form to winter-form by affecting the cuticle thickness and chitin content. Subsequently, we demonstrated that *CcTRPM* functions as a temperature receptor to regulate this transition. In addition, miR-252 was identified to mediate the expression of *CcTRPM* to involve in this morphological transition. Finally, we found *CcTre1* and *CcCHS1*, two rate-limiting enzymes of insect chitin biosyntheis, act as the critical down-stream signal of *CcTRPM* in mediating this behavioral transition. Taken together, our results revealed that a signal transduction cascade mediates the seasonal polyphenism in *C. chinensis*. These findings not only lay a solid foundation for fully clarifying the ecological adaptation mechanism of *C. chinensis* outbreak, but also broaden our understanding about insect polymorphism.

Keywords: *Cacopsylla chinensis*, miR-252, *CcTRPM*, polyphenism, low temperature

Introduction

Currently, global climate change is the most important environmental problem facing with mankind, and also one of the most complex challenges in the 21st century. Insects, as the largest animal population on the earth, adapt to the complex and changeable external environment by displaying polyphenism, thus achieving the purpose of survival and reproduction (Simpson et al., 2011). Insect polyphenism is the phenomenon allows them within a given genotype to produce two or more distinct phenotypes under the challenges posed by environmental variability via beneficial shifts in morphology, behavior, or physiology (Cridge et al., 2015). Polyphenism is commonly observed in many insect species, for examples: the solitary and gregarious phases of *Locusta migratoria* (Ma et al., 2011), the short-winged and long-winged morph of *Nilaparvata lugens* (Xu et al., 2015), the wingless and winged aphid of *Acyrthosiphon pisum* (Vellichirammal et al., 2017), and the catkin and twig morphs in caterpillars of the moth *Nemoria arizonaria* (Simpson et al., 2011). With the global climate problems are increasingly prominent, the study of insect polyphenism has become a new hotspot in insect ecology, epigenetics and developmental biology.

Pear psylla is a serious pest of pear trees worldwide, including *Cacopsylla chinensis* (Yang & Li), *Psylla Betulaefoliae*, *Psylla Pyri*, and so on (Butt and Stuart, 1986; Wei et al., 2020). *C. chinensis*, belongs to Hemiptera: Psyllidae, which exclusively feeds on pear trees, harms the young shoots and leaves with adult and nymph, and secretes a large amount of honey dew to breed coal pollution bacteria of *Gloeodes pomigena* (Wei et al., 2020). It is also an important vector of the destructive disease of pear trees, *Erwinia amovora*, and currently one of the key pests in the major pear production areas in many East Asian countries, including China and Japan (Hildebrand et al., 2010; Ge et al., 2019). In most pear production areas of China, the summer-form of *C. chinensis* are usually present from April to September, whereas winter-form of *C. chinensis* are present during the rest of the year (Ge et al., 2019; Wei et al., 2020). The summer-form has lighter body color and stronger activity ability, and causes more serious damage compare with winter-form. For better adapt to the harsh environmental conditions, the eggs of summer-form develop to the winter-form before the pear fallen leaves. The winter-form has brown to dark brown body color and larger body size, but has the weaker activity ability and stronger resistance ability compare with summer-form. With the gradual increase of temperature in early spring, the winter-form lays eggs at the tender buds of pear trees and then develop into summer-form (Ge et al., 2019; Tougeron et al., 2021). Hence, the transition between summer-form and winter-form is a significant ecological strategy for *C. chinensis* to avoid adverse environmental conditions and then burst into disaster, which has prominence biological and ecological significance. The seasonal polyphenism of summer-form and winter-form in *C. chinensis* has been recognized for many years and could be induced by low temperature and short day (Oldfield, 1970; Tougeron et al., 2021), but until recently no molecular mechanism had been advanced.

Temperature is a significant factor limiting the geographic ranges of species, which determines the distribution and diffusion area of species. As a type of small poikilothermic animal, insect is sensitive to temperature changes and temperature stress response is one of the most conservative mechanism to resist extreme environment (Teets et al., 2023). Different environmental conditions affect the polyphenism of many kinds of insects, for examples, wing dimorphism of Hemiptera *Schizaphis graminum* (An et al., 2012), diapause of Lepidoptera

Bombyx mori (Tsuchiya et al., 2021) and Coleoptera *Colaphellus bowringi* (Guo et al., 2021). Under the low temperature conditions, insects can improve cold tolerance by regulating their internal energy metabolism and external exoskeleton system. Such as: darken their cuticles with melanin (Fedorka et al., 2013), thickened wax layer or chorion (Kreß et al., 2016), and store more lipids to increase energy supply and increase the accumulation of antifreeze protective substances (Terblanche et al., 2011). However, studies about how insect temperature receptor response to temperature change and then activates the downstream signal molecules to regulate the polyphenism have been very limited.

Transient receptor potential (TRP) channel family gene was firstly found in *Drosophila melanogaster* (Minke et al., 1975). The TRP channel genes involved in temperature sensing are called "thermo-sensitive TRP" or "temperature receptor" (Lee et al., 2005). In mammals, there are six thermo-sensitive TRP receptor genes, of which TRPV1-4 mainly feel moderate high temperature (Venkatachalam and Montell, 2007) and TRPM8 can be activated by low temperature (8°C-28°C) or cooling substances, such as menthol and borneol (Peier et al., 2002). The activation mode is mainly due to the depolarization of cell membrane caused by the influx of Ca^{2+} (McKemy et al., 2002). Presently, researches on the function of temperature receptor gene TRP were mainly focused on some model insects, but very few on the agricultural pests. For example, *D. melanogaster TRPM* is highly expressed in dendritic sensory neurons and can sense cold stimulation (Turner et al., 2016). In *B. mori*, high temperature receptor *BmTRPA1* regulates the diapause of offspring eggs by acting on the neuroendocrine hormone signal of GABAergic-GnRH/Crz-DH (Sato et al., 2014; Tsuchiya et al., 2021). However, studies on agricultural insects, such as *Apolygus lucorum* (Fu et al., 2016), *N. lugens* (Wang et al., 2021a), *Bemisia tabaci* (Dai et al., 2018), and *Tuta absoluta* (Wang et al., 2021b), also only focused on the identification of the related temperature receptor gene TRPs and its correlation with temperature, no detailed molecular mechanism were reported. In agricultural insects, members of TRPA subfamily are mainly responsible for answering the high-temperature stimulation (Tracey et al., 2003; Neely et al., 2011), while members of TRPM subfamily are mainly involved in low-temperature stimulation as temperature receptors (Rosenzweig et al., 2008; Turner et al., 2016). Temperature significantly affected the annual generations, adult survival rate, hibernation period and egg laying period of *C. chinensis* (Butt and Stuart, 1986). Our preliminary research results found that low temperature is the key factor to induce the transition from summer-form to winter-form in *C. chinensis*. Therefore, we speculated that *TRPM*, functions as a temperature receptor gene, may participate in the transition from summer-form to winter-form in response to low temperature, but the specific molecular mechanism needs to be further explored.

MicroRNAs (miRNAs), a class of non-coding RNA molecules, were encoded by endogenous genes in a length of about 18-25 nt. They mainly regulate many life processes, including cell differentiation, organ development, cell apoptosis, biological rhythm and metamorphosis development in animals and plants at the post-transcriptional level by inhibiting the translation process of target genes or degrading the mRNA of target genes (Asgari, 2013). In recent years, more and more studies reported that miRNAs are involved in regulating the insect polymorphism, such as the caste differentiation of honeybees, the phenotypic plasticity of *L. migratoria* and the wing pleomorphism of *N. lugens* (Liu et al., 2012; Yang et al., 2014; Ye et al., 2019). In addition, miRNAs also play important roles in insect adaptation to temperature stress. For examples, miR-7 and miR-8 involved in the process of temperature adaptation of *D. melanogaster* (Kennell et al.,

114 2012). MiRNAs were also found in responding to low temperature stress in rice water weevil
115 (*Lissorhoptrus oryzophilus*) and gall midge (*Epiblema Scudderiana*) (Yang et al., 2017a; Lyons et
116 al., 2015). There were also reported that miR-204 targeted *TRPM3* to regulate mammalian eye
117 development (Shiels, 2020), and miR-135a targeted *TRPC1* to participate in podocyte injury
118 (Yang et al., 2017b). Here, we screened and validated miR-252, a miRNA whose expression was
119 down-regulated under low temperature, negatively targeted *CcTRPM* to modulate the transition
120 from summer-form to winter-form by acting on the cuticle thickness and cuticle chitin content.
121 Chitin biosynthesis signal was also proved to involve in the transition from summer-form to
122 winter-summer in response to *CcTRPM* and miR-252. Our work not only promotes the
123 comprehensive understanding of the adaptation mechanism for *C. chinensis* outbreak at the
124 physiological and ecological level as well as the insect polymorphism, but also helpful in
125 identifying potential target genes in pest control through blocking temperature adaptation of pests.

126 **Results**

127 **Low temperature induced the transition from summer-form to winter-form in *C. chinensis***

128 *C. chinensis* was displayed as seasonal polyphenism along with seasonal changes: the
129 summer-form and the winter-form. The significant differences in morphological characteristics are
130 as following: (1) Eggs are long oval shape with a thin tip and a blunt end. Eggs of summer-form
131 are milky white at the initial stage and gradually become yellow white at the later stage (Figure
132 1A). Eggs of winter-form are mostly yellowish brown or orange (Figure 1A'). (2) The nymph has
133 five instars and its body size is gradually increasing with age. The body of the newly hatched
134 nymph is oval and the compound eyes are red. The 1st instar nymph of summer-form is light
135 yellow and transparent (Figure 1B). The 3rd and 5th instar nymphs of summer-form are
136 yellow-green or blue-yellow, and the wing buds are oblong, protruding and sticking to both sides
137 of the body (Figure 1C and 1D). The 1st instar nymph of winter-form has many black stripes on
138 the chest back plate, and the end of the abdomen and back are black (Figure 1B'). The 3rd and 5th
139 instar nymphs of winter-form are overall black brown, with dark brown stripe on the left and right
140 sides of each section on the chest and back of the abdomen, and the end of the abdomen and back
141 becomes a large piece with black brown color (Figure 1C' and 1D'). (3) The antennae of adults
142 are filamentous with 10 nodes, and the front wings are translucent and oblong. The body color of
143 summer-form adult is green or yellow-green with yellow-brown stripes on the shield of the chest
144 and back plate, and no stripes on the wings (Figure 1E). The body color of winter-form adult is
145 brown or dark brown, with dark brown stripes on the whole body, and clearly brown stripes on the
146 rear edges of the front wings (Figure 1E').

147 To clarify the effect of temperatures on the transition from summer-form to winter-form, the
148 newly-hatched 1st instar summer-form nymphs were treated with four different temperatures
149 (25°C, 20°C, 15°C, and 10°C). The results indicated that all the survived treated nymphs develop
150 to the 3rd instar summer-form nymphs at 25°C, approximately 17% and 40% of survived treated
151 nymphs develop to the 3rd instar winter-form nymphs at 20°C and 15°C, but all the survived
152 treated nymphs develop to the 3rd instar winter-form nymphs at 10°C (Figure 1F). It meant that
153 low temperature (especially 10°C) was the key environment factor to induce the transition from
154 summer-form to winter-form and 10°C was selected for the following study. In addition, two
155 cooling agents, menthol and borneol, were also used to mimic the low temperature effect of 10°C.

156 We observed that about 49% and 37% of the survived treated nymphs develop to the 3rd instar
157 winter-form nymphs after menthol and borneol treatment at 25°C, respectively (Figure 1G).
158 To further explore the differences between summer-form and winter-form nymphs, cuticle
159 thicknesses and cuticle chitin content were determined. The ultrastructure results of transmission
160 electron microscopy assays showed that cuticle thicknesses of 3rd instar winter-form (about 3.86
161 μm) were obviously higher than 3rd instar summer-form (about 1.82 μm) (Figure 1H and 1I). We
162 also found that winter-form nymphs exhibited higher chitin level in cuticle compared to the
163 summer-form nymphs by using the WGA-FITC staining and chitin content determination (Figure
164 1J and 1K). Taken together, these findings demonstrated that low temperature of 10°C induced the
165 transition of summer-form to winter-form by affecting the cuticle thicknesses and cuticle chitin
166 content.
167
168 ***CcTRPM* is a conventional cold-sensing TRP channel activated by 10°C in *C. chinensis***
169 A cDNA fragment, which was putatively encoded a cold-sensing TRPM channel gene, was
170 identified as *CcTRPM* from *C. chinensis*. The full-length sequence of *CcTRPM* was amplified and
171 verified by RT-PCR with specific primers (Table S1) and sequencing. Sequence analysis
172 displayed that the ORF of *CcTRPM* was 4566 bp with a 455 bp 3'UTR and encoded a deduced
173 polypeptide of 1521 amino acids with six transmembrane domains. Multiple alignment analysis of
174 the amino acid sequence indicated that the transmembrane domains of *CcTRPM* shared very high
175 amino acid identity with TRPM sequences from other five selected insect species (Figure S1A).
176 As shown in Figure S1B, phylogenetic analysis revealed that insects TRPM and mammals TRPM
177 belong to different branches in evolution. *CcTRPM* was most closely related to the *DcTRPM*
178 homologue (*Diaphorina citri*, XP_017299512.2) in evolutionary relationship, and both of them
179 belong to important Hemiptera pests of fruit trees. The potential tertiary protein structure of
180 *CcTRPM* was constructed with the online server Phyre[2] and modified with PyMOL-v1.3r1
181 software, and the conserved ankyrin repeats (ANK) and six transmembrane domains were
182 identified (Figure 2A).
183 The results of temperature treatment indicated that the mRNA expression of *CcTRPM* was
184 obviously induced by 10°C treatment at 1, 2, 3, 6, and 10 days compared with 25°C treatment by
185 qRT-PCR (Figure 2B, Figure S2F). It is well known that the TRPM subfamily channels in
186 vertebrates are activated by a variety of chemical compounds, including menthol (Peier et al.,
187 2002). We therefore attempted to identify chemical compounds that either activate or inhibit
188 *CcTRPM*. qRT-PCR results revealed that menthol treatment with all three concentrations
189 significantly increased the mRNA expression of *CcTRPM* and antagonist (HY-112430,
190 MedChemExpress, Shanghai, China) treatment with all three concentrations markedly reduced
191 *CcTRPM* transcription (Figure S2G-S2H). To further confirm *CcTRPM* is a cold-sensing TRP
192 channel gene, fluorescence detection of Fluo-4 AM and Ca^{2+} imaging was performed to determine
193 whether CcTRPM-expressing cells increased intracellular Ca^{2+} concentration upon 10°C treatment
194 and menthol treatment. The results of fluorescence detection of Fluo-4 AM indicated that there
195 was no change of Ca^{2+} concentration in CcTRPM-expressing cells was treated with DMSO, but a
196 clear increase of Ca^{2+} concentration was observed when treated with menthol which was similar
197 with the trend of pcDNA-expressing cells was treated with the positive control of ionomycin
198 (Figure 2C). The effect of 10°C and menthol on *CcTRPM* was further tested using Ca^{2+} imaging
199 and showed that both 10°C and menthol treatment obviously elevated intracellular Ca^{2+} levels in

200 CcTRPM-expressing cells (Figure 2D, S2I). We therefore concluded that *CcTRPM* is a
201 cold-sensitive ion channel activated by 10°C low temperature and menthol.
202
203 ***CcTRPM* modulated the transition from summer-form to winter-form of *C. chinensis* in**
204 **response to low temperature**
205 Temporal expression profiles by qRT-PCR revealed that *CcTRPM* mRNA expressed in all
206 determined stages, with the highest expression level in the 1st instar nymph, and showed a
207 decreased trend from 2nd instar nymph to adult 1 day (Figure 2E). The FISH results also indicated
208 that *CcTRPM* mRNA has a greatest expression level in the 1st instar nymph and relative lower
209 expression in the 3rd and 5th instar nymph (Figure 2F).
210 To study whether *CcTRPM* modulated the transition from summer-form to winter-form of *C.*
211 *chinensis*, the newly-hatched 1st instar nymphs of summer-form were fed with dsCcTRPM or
212 dsEGFP. For the RNAi efficiency under 10°C condition, feeding of dsCcTRPM reduced the
213 transcription level of *CcTRPM* by about 61% and 62% compare to dsEGFP feeding at 3 d and 6 d
214 by qRT-PCR (Figure S3A), and decreased the CcTRPM-Cy3 signal at 6 d by FISH (Figure S3B).
215 Both results of cuticle ultrastructure and cuticle chitin content determination showed that cuticle
216 thicknesses (about 1.97 μm) and cuticle chitin content of dsCcTRPM-treated nymphs were
217 markedly lower than dsEGFP-treated nymphs (about 3.71 μm) under 10°C condition (Figure 2G
218 and 2H). Additionally, dsCcTRPM feeding and *CcTRPM* antagonist treatment both significantly
219 decreased the transition percent from summer-form to winter-form, but menthol feeding only
220 partially rescued the transition percent and morphological phenotype under dsCcTRPM feeding
221 (Figure 2I and 2J). To exclude the effect of *CcTRPM* itself on the transition percent and nymph
222 development, we also performed the RNAi assays under 25°C condition. After successfully
223 interfered the mRNA expression of *CcTRPM*, the nymph development and morphological
224 phenotype were not affected compared to the dsEGFP treatment (Figure S3C-S3D). Together,
225 these findings indicated that *CcTRPM* functions as an essential molecular signal to modulate the
226 transition from summer-form to winter-form of *C. chinensis* in response to low temperature.
227
228 **Confirming of miR-252 targeted *CcTRPM***
229 To explore the regulation mechanism of *CcTRPM* at the post-transcriptional level, two
230 software programs of miRanda and Targetscan were used to predict the potential miRNAs. There
231 are four miRNAs (miR-252, miR-5728, PC-3p-173924, and PC-3p-137568) were predicted to
232 have the corresponding target-binding sites with the 3'UTR of *CcTRPM* (Figure 3A and S4A).
233 miR-252 showed the opposite expression patterns with *CcTRPM* after 25°C and 10°C treatments
234 (Figure 2B and 3B). To further determine whether miR-252 specifically targeted *CcTRPM*, the
235 following four experimental approaches were performed: (1) The dual-luciferase reporter assays
236 were carried out by cloning a 419 bp 3'UTR fragment of *CcTRPM* containing the predicted target
237 binding sites of the miRNAs. The relative luciferase activities were obviously decreased when the
238 agomir-252 and CcTRPM-3'UTR-pmirGLO were cotransfected, while the activity recovered to
239 the control when using the mutated 3'UTR sequence without the binding sites of miR-252 (Figure
240 3C). However, the relative luciferase activities were no change when the construct of
241 CcTRPM-3'UTR-pmirGLO was cotransfected with the agomir of other three miRNAs,
242 respectively (Figure S4B). (2) An RNA immunoprecipitation assay indicated that the transcripts of
243 *CcTRPM* and miR-252 increased 6.35-fold and 9.21-fold from the agomir-252 feeding nymphs of

244 the Ago-1 antibody-mediated RNA complex compared to an IgG control, separately (Figure 3D
245 and S5). (3) FISH results showed that *CcTRPM* and miR-252 were co-expressed in the nymphs
246 and displayed an opposite expression trend along with the increasing instar (Figure 3E). (4)
247 qRT-PCR results indicated that agomir-252 feeding significantly inhibited *CcTRPM* mRNA
248 expression and antagomir-252 feeding markedly increased *CcTRPM* mRNA expression compare
249 to their controls, separately (Figure 3F). These data together confirmed that miR-252 directly
250 targeted *CcTRPM*.
251
252 **miR-252 mediated the transition from summer-form to winter-form in *C. chinensis* by**
253 **suppressing *CcTRPM***
254 To test the efficiency of agomir-252, 1st instar nymphs of summer-form were fed with
255 agomir-252 under 10°C condition. qRT-PCR results showed that miR-252 expression was both
256 significantly increased after agomir-252 treatment at 3 d and 6 d (Figure 4A). To further clarify
257 the relationship between *CcTRPM* and miR-252, we determined miR-252 expression after
258 dsCcTRPM treatment under 10°C condition. Interestingly, miR-252 expression was dramatically
259 inhibited after successful interference of *CcTRPM* at 3 d and 6 d (Figure 4B). This result implied
260 that up-regulation of *CcTRPM* expression may have a positive feedback to miR-252 expression in
261 response to 10°C temperature.
262 To deeply decipher the role of miR-252 in the transition from summer-form to winter-form,
263 1st instar nymphs of summer-form were fed with agomir-NC or agomir-252 under 10°C condition.
264 Results of cuticle ultrastructure indicated that cuticle thickness of agomir-252 treated nymphs
265 (about 1.85 μm) was markedly lower than agomir-NC treated nymphs (about 3.70 μm) (Figure 4C
266 and 4D). Both WAG-FITC staining and chitin content determination revealed that cuticle chitin
267 content of agomir-252 treated nymphs were obviously lower than agomir-NC treated nymphs
268 (Figure 4E and 4F). Moreover, agomir-252 feeding significantly decreased the transition percent
269 from summer-form to winter-form, but antagomir-252 feeding rescued the defect of transition
270 percent and morphological phenotype under dsCcTRPM treatment (Figure 4G, Table S2, and 4H).
271 To further evaluate the effect of agomir-252 under 25°C condition, we determined *CcTRPM*
272 expression and observed the nymph development after agomir-252 feeding. As expected,
273 *CcTRPM* expression was still significantly decreased after agomir-252 feeding (Figure S6C), but
274 the nymph development and morphological phenotype were not affected by agomir-252 treatment
275 compared to the agomir-NC treatment (Figure S6D). Above all, these results displayed that
276 miR-252 mediated the transition from summer-form to winter-form in *C. chinensis* by suppressing
277 *CcTRPM* via affecting the cuticle thickness and cuticle chitin content.
278
279 **Chitin biosynthesis signaling involved in the transition from summer-form to**
280 **winter-summer of *C. chinensis* in response to low temperature and *CcTRPM***
281 Since cuticle thickness and cuticle chitin content were obviously affected by dsCcTRPM
282 treatment and agomir-252 treatment, we speculated that chitin biosyntheis signaling pathway
283 participated in the transition from summer-form to winter-form. To demonstrate this hypothesis, a
284 total of 14 transcripts corresponding to 8 genes involved in chitin biosyntheis were identified in *C.*
285 *chinensis*, with several genes were present in two or more paralogous forms (Figure 5A). Next, we
286 used qRT-PCR to determine the expression profiles of these 14 chitin biosyntheis transcripts after
287 25°C and 10°C treatments at 3 d, 6 d, and 10 d. Based on the relative gene expression in the heat

288 map, we found that the expression of 13 transcripts exhibited overall up-regulation under 10°C
289 condition at 3 d, 6 d, and 10 d compared to those under 25°C condition, while levels for CcUAP2
290 were almost unchanged (Figure 5B).
291 Subsequently, we used RNAi to further uncover the impact of chitin biosyntheis genes in the
292 transition from summer-form to winter-form. Compared with dsEGFP feeding control, only
293 knockdown of *CcTre1* and *CcCHS1* obviously decreased the transition percent from summer-form
294 to winter-form, but not by knockdown of the remaining transcripts (Figure 5C). To further dissect
295 the roles of *CcTre1* and *CcCHS1*, cuticle thickness and cuticle chitin content were also determined.
296 Compared with dsEGFP feeding control, knockdown of *CcTre1* and *CcCHS1* markedly reduced
297 the cuticle thickness and cuticle chitin content (Figure S7C-S7D, 5D-5F), which were similar with
298 dsCcTRPM feeding and agomir-252 treatment. To confirm whether *CcTre1* and *CcCHS1* function
299 as the downstream of *CcTRPM* and miR-252, we next determine the expression of *CcTre1* and
300 *CcCHS1* after *CcTRPM* knockdown and agomir-252 feeding. qRT-PCR results indicated that
301 *CcTRPM* knockdown and agomir-252 feeding were both obviously reduced the mRNA expression
302 of *CcTre1* and *CcCHS1* at 3 d and 6 d, respectively (Figure 5G-5J). These phenotypic and
303 molecular data suggested that chitin biosynthesis signaling involved in the transition from
304 summer-form to winter-summer of *C. chinensis* in response to low temperature and *CcTRPM*.

305 **Discussion**

306 Polyphenism offers the opportunity for insects to deploy different phenotypes generated from
307 the same genome to best suit the extreme environmental changes (Simpson et al., 2011). In recent
308 years, studies on insect polyphenism have mainly focused on the molecular regulation by
309 endocrine hormones, neuropeptides, and neurotransmitters, while the regulation mechanism by
310 external environmental factors remains poorly understood. For examples, ecdysone signaling and
311 insulin/IGF signaling pathway regulated the wing polyphenism of pea aphid (Vellichirammal et al.,
312 2017) or planthoppers (Zhang et al., 2022), neuropeptide F was essential for shaping locomotor
313 plasticity in locust (Hou et al., 2017), and dopamine metabolic pathway modulated the behavioral
314 phase changes of the migratory locust (Ma et al., 2011). Temperature is important in defining the
315 distribution of insects, but how it activates the temperature receptor and then regulates
316 polyphenism need further deeply study. Here, we firstly demonstrated that the transition from
317 summer-form to winter-form in *C. chinensis* was "temperature-dependent pattern", and low
318 temperature of 10°C completely induced this transition. Just like people wear more clothes in the
319 winter, we also proved that 10°C induced the summer-form change to winter-form by increasing
320 the cuticle thickness and cuticle chitin content. Several similar phenotype changes have been
321 reported in other insects: the cricket of *Allonemobius socius* exhibited darker cuticles to improve
322 thermo-regulation in colder environments (Fedorka et al., 2013), the mosquito of *Aedes albopictus*
323 increased the thickness of the egg middle serosa cuticle and wax layer as an adaptation strategy for
324 cold acclimation (Kreß et al., 2016).
325 TRPM8, a member of the TRP family, has been reported as the principal sensor of
326 environmental cold in mammals (Peier et al., 2002). As a kind of poikilothermic animals, insects
327 also have an evolutionarily conserved TRPM gene which is homologous to mammalian
328 temperature receptor of TRPM8 (Venkatachalam and Montell, 2007). In this study, we identified a
329 classical TRPM gene in *C. chinensis* which was designated as *CcTRPM* and functioned as a low

330 temperature receptor by using qRT-PCR and calcium imaging. After knockdown of *CcTRPM* by
331 feeding dsCcTRPM, the treated nymphs displayed thinner cuticle thickness and less cuticle chitin
332 content compared with the control of dsEGFP treatment under 10°C condition. In addition,
333 *CcTRPM* knockdown by RNAi or *CcTRPM* antagonist feeding both caused obvious defect of the
334 transition percent from summer-form to winter-form, but this defect could be partially rescued by
335 a cooling agent menthol treatment. To exclude the developmental defect or genetic background,
336 we also knocked down *CcTRPM* under 25°C condition, and not found any death defect and cuticle
337 defect. These results were the first report about *CcTRPM* was essential for insect polyphenism in
338 response to low temperature. Until now, the researches about TRPM on other agricultural insects
339 only focused on the description of its correlation with temperature, but no deeply molecular
340 function was reported (Fu et al., 2016; Wang et al., 2021a). Therefore, the molecular regulation
341 mechanism of *CcTRPM* in response to low temperature needs further study. TRPV ion channel
342 has been reported to function as a heat-activated receptor in mammals by David Julius (Caterina et
343 al., 1997; Cao et al., 2013). So, TRPV is supposed to function as a heat-activated receptor in *C.*
344 *chinensis*, and it is also worthy to explore whether it induces the transition from winter-form to
345 summer-form in the future.
346 miRNAs played significant roles in insect polyphenism and cold acclimation. For example,
347 miR-34 and miR-9b mediated the wing dimorphism of *N. lugens* (Ye et al., 2019) and *A. citricidus*
348 (Shang et al., 2020), miR-133 inhibited behavioral aggregation by controlling dopamine synthesis
349 in *L. migratoria* (Yang et al., 2014), and miR-31-5p via asc-C9 to regulate cold acclimation in
350 *Monochamus alternatus* (Zhang et al., 2020). Here, we demonstrated that a key regulator,
351 miR-252, targets *CcTRPM* via a negative feedback loop to control the transition from
352 summer-form to winter-form in response to low temperature. Interestingly, RNAi-mediated
353 knockdown of *CcTRPM* also decreased the expression of miR-252. This result implied that
354 up-regulation of *CcTRPM* in response to low temperature may be have a feedback to miR-252,
355 then miR-252 inhibits the expression of *CcTRPM* under low temperature condition to avoid its
356 excessive expression. Upon miR-252 agomir feeding, the treated nymphs showed thinner cuticle
357 thickness and less cuticle chitin content compared with the control of agomir-NC feeding under
358 10°C condition. Besides, miR-252 antagomir feeding could rescue the transition percent defect
359 and morphological phenotype defect caused by *CcTRPM* knockdown. These results were the first
360 report about miR-252 functions as the up-stream regulator to control the transition from
361 summer-form to winter-form in response to low temperature via acting on the insect cuticle
362 thickness and cuticle chitin content. Similar result was reported in *Daphnia pulex*, miR-252 might
363 increase cadmium tolerance by switching cellular growth and cuticle protein pathways to
364 detoxification processes (Chen et al., 2016). In *Leptinotarsa decemlineata*, 42 differentially
365 expressed miRNAs were identified following cold exposure including miR-9a-3p, miR-210-3p,
366 miR-276-5p and miR-277-3p (Morin et al., 2017). Therefore, the regulatory network of miRNAs
367 is need further investigating in the transition between two phases in *C. chinensis*, especially
368 transboundary miRNAs from host plant.
369 Insect cuticle serves as a protective barrier and plays significant roles in supporting the body,
370 resisting the adverse environmental conditions, preventing predators from predation, and
371 preventing pathogens from invading (Evans and Sanson, 2005; Vargas et al., 2014). Chitin as an
372 extremely important structural component of insects and represents up to 60% of the dry weight in
373 some species (Richards, 1978). Many studies have reported that insect cuticles are essential for

374 cold acclimation (Fedorka et al., 2013; Kreß et al., 2016). In this study, cuticle thickness and
375 cuticle chitin content were the major differences between summer-form and winter-form. We have
376 demonstrated that *CcTRPM* and miR-252 function as the up-stream signaling to mediate the
377 transition from summer-form to winter-form in response to low temperature via affecting the
378 cuticle thickness and cuticle chitin content. Therefore, it is necessary to study whether chitin
379 biosynthesis pathway acting as the down-stream signaling in this transition. The de novo
380 biosynthesis of chitin has eight enzymatic steps, including 1 Trehalose, 2 enzymes in Glycolysis, 4
381 enzymes in Hexosamine pathway, and 1 Chitin synthesis (Doucet and Retnakaran, 2012). Further
382 RNAi results showed that two rate-limiting enzyme genes, *CcTre1* and *CcCHS1*, play essential
383 roles in the transition from summer-form to winter-form in response to low temperature and affect
384 the cuticle thickness and cuticle chitin content. Glycolysis and hexosamine pathway are two
385 complex cellular metabolic processes within organisms. We supposed that there are two reasons
386 for not all of these steps were required: (1) the function of some enzymes may be replaced or
387 supplemented by other enzymes, for examples, function of hexokinase and glucokinase was
388 similar. (2) The reason for no obviously phenotypic defects might be cause by insufficient
389 interference efficiency of RNAi. So, it's worth to further study the functions of these chitin
390 biosynthesis enzymes by CRISPR-Cas9 in future. In addition, *CcTRPM* knockdown and miR-252
391 agomir feeding both markedly decreased the mRNA expression of *CcTre1* and *CcCHS1*. These
392 results proved our hypothesis and were the first report that chitin biosynthesis pathway functions
393 as the down-stream signaling to control the transition from summer-form to winter-form in *C.*
394 *chinensis*.
395 In summary, this study reported a novel signaling pathway of low
396 temperature-miR-252-*CcTRPM* acting on cuticle chitin biosynthesis genes to mediate the
397 transition from summer-form to winter-form in *C. chinensis*. We proposed a working model to
398 describe this novel mechanism in Figure 6. Under 25°C condition, the expression of temperature
399 receptor *CcTRPM* was depressed by miR-252, so the 1st instar nymphs of summer-form normally
400 developed into 3rd instar nymphs of summer-form. However, under 10°C condition, low
401 temperature greatly activated the expression of *CcTRPM*, but miR-252 functioned as a negative
402 feedback regulator to mediate *CcTRPM* expression to avoid its excessive expression in response to
403 low temperature. Then, *CcTRPM* obviously improved the expression of two rate-limiting enzyme
404 genes from cuticle chitin biosynthesis pathway, *CcTre1* and *CcCHS1*, to increase cuticle thickness
405 and raise cuticle chitin content. Lastly, the 1st instar nymphs of summer-form developed to 3rd
406 instar nymphs of winter-form as an ecological adaptation strategy under low temperature stress.
407 Future researches will focus on the following directions: (1) Whether and how transboundary
408 miRNAs and hormones from host plant involve in the transition from summer-form to
409 winter-form in *C. chinensis*. (2) How neuropeptides and endocrine hormones response to low
410 temperature and *CcTRPM* to mediate the transition from summer-form to winter-form in *C.*
411 *chinensis*.

412 **Materials and Methods**

413 **Insects and host plants**

414 The summer-form and winter-form colonies of *C. chinensis* (Yang & Li) were initiated
415 collected in June and December 2018 from a pear orchard in Daxing district, Beijing, China,

416 respectively. These two populations are now reared in the integrated pest management (IPM)
417 laboratory of China Agricultural University. The summer-form population was raised in growth
418 chambers at 25 ± 1°C under a photoperiod of 12L: 12D with 65 ± 5% RH (relative humidity). The
419 feeding conditions of winter-form population were raised at 10 ± 1 ° C under a photoperiod of 12L:
420 12D with 25 ± 5% RH. Unless otherwise specified, the photoperiod of all the following different
421 temperature treatments is 12L: 12D.
422 Host plants were 2-3 years old Korla fragrant pear seedlings with a height of 60-100 cm
423 under conventional water and fertilizer management.
424
425 **Different temperatures and cooling agents induced the transition from summer-form to**
426 **winter-form**
427 For different temperatures treatment, the newly-hatched 1st instar summer-form nymphs
428 (within 12 h) were transferred to the young vegetative shoots of healthy Korla fragrant pear
429 seedlings at four different temperatures (25°C, 20°C, 15°C, and 10°C) by using a fine brush. Then,
430 observed the morphological characteristics every two days, and counted the number of
431 summer-form and winter-form individuals according to the body color and external characteristics
432 until the 3rd instar. Each treatment was performed with three independent biological replications
433 of at least 30 nymphs for each biological replication.
434 Menthol (HY-N1369) was purchased from MedChemExpress LLC (Shanghai, China) and
435 borneol (420247) was bought from Sigma-Aldrich LLC (Saint Louis, USA) (Figure S2A-S2B)
436 (Peier et al., 2002; Turner et al., 2016). For the treatment of different cooling agents, feeding setup
437 through a pear leaf was used as previously described in *Aphis citricidus* with minor adjustment
438 (Shang et al., 2020). Briefly, a stem with a fresh pear leaf was inserted into a sterile PCR tube of
439 250 μL containing 200 μL of menthol (1 mg/mL) or borneol (0.1 mg/mL). Then, the PCR tube
440 with leaf was transferred to a 50 mL sterile plastic tube, termed as stem-leaf device. Finally,
441 transferred the newly-hatched 1st instar summer-form nymphs (within 12 h) into the stem-leaf
442 device, observed the morphological characteristics every two days, and counted the number of
443 summer-form and winter-form individuals according to the body color and external characteristics
444 until the 3rd instar under 25°C. Each treatment was performed with three independent biological
445 replications of at least 30 nymphs for each biological replication.
446
447 **Transmission electron microscopy assay of cuticle**
448 To analyze the difference of nymph cuticle ultrastructure and thickness of thorax between
449 different samples, transmission electron microscopy was used as previously described (Ekino et al.,
450 2017; Ge et al., 2019). Briefly, the body samples without head were firstly fixed in 4%
451 polyformaldehyde (PFA) for 48 h and followed by post-fixation in 1% osmium tetroxide for 1.5 h.
452 Next, the samples were dehydrated in a standard ethanol/acetone series, infiltrated and embedded
453 in spurr resin embedding medium. Then, the superthin sections (-70 nm) of thorax were cut and
454 stained with 5% uranyl acetate followed by Reynolds' lead citrate solution. Finally, the sections
455 were observed, photographed and measured under a Hitachi HT7800 transmission electron
456 microscope operated at 120 kv. Five nymphs were used for each sample.
457
458 **Cuticle chitin staining assay with WGA-FITC and determination of cuticle chitin content**

459 Previous studies have demonstrated that cuticle thickness and hardness are important
460 parameters for adapting to environment and natural enemies (Evans and Sanson, 2005). Therefore,
461 cuticle chitin staining with WGA-FITC (Cat# F8520, Solarbio, Beijing, China) and cuticle chitin
462 content were measured to analyze the difference between the summer-form and winter-form
463 nymphs, or dsRNA treatment and miRNA agomir treatment. For the WGA-FITC staining, nymph
464 samples were firstly fixed with 4% PFA for 48 h and dehydrated with a series of sucrose solution
465 with varied concentrations (10% for 4 h, 20% for 4 h, 30% for 12 h), then rinsed three times for 15
466 min per rinse with sterile PBS buffer. The dehydrated samples were gradually embedded in
467 Tissue-Tek O.C.T. compound (Cat# 4583, SAKURA, Ningbo, China) after the pre-embedding
468 stages under -25°C. The ultra-thin sections (approximately 70 nm thickness) of embedded material
469 were cut using Leica freezing ultra-cut microtome (CM1850, Leica, Weztlar, Germany). The
470 sections were stained with WGA-FITC (50 μg/mL) and DAPI (10 μg/mL) for 15 min and then
471 rinsed three times for 15 min per rinse with sterile PBS buffer as previously described (Farnesi et
472 al., 2012; Xie et al., 2022). Fluorescence images were acquired using a Leica SP8 confocal
473 microscopy (Weztlar, Germany).
474 For the determination of cuticle chitin content, chitin Elisa kit (Cat# YS80663B, Yaji
475 Biotechnology, Shanghai, China) was used according to the manufacturer's instruction. In short,
476 each 50 nymphs for one sample were homogenized in 0.2 mL distilled water using an electric
477 homogenizer. The testing samples and standard samples were hatched in enzyme-labeled plates at
478 37°C for 30 min, separately. The washing buffer was used to rinse the enzyme-labeled plates five
479 times for 30 s per time. Then, enzyme labeling reagent was added to the plates for hatching and
480 washing. Finally, chromogenic agent A solution and B solution were mixed in holes for coloration
481 at 37°C and protect from light. The absorbance (OD value) of each hole was measured at 450nm
482 wavelength and zeroed with a blank hole.
483
484 **Sequence characterization of *CcTRPM***
485 The GenBank accession number of *CcTRPM* was OQ658558. The putative transmembrane
486 domains of CcTRPM were identified by an online software of SMART (a Simple Modular
487 Architecture Research Tool). The tertiary protein structures of *CcTRPM* was predicted with online
488 server Phyre[2] (http://www.sbg.bio.ic.ac.uk/phyre2/html/page.cgi?id=index) and modified with
489 PyMOL-v1.3r1 software. BLASTP in NCBI database was used to search the homologous protein
490 sequences of *CcTRPM* from insects and mammals of different species, including 5 Hemiptera
491 insects, 2 model insects, and 2 mammals. Multiple alignments of the amino acid sequences for
492 *CcTRPM* with other homologies was performed using DNAman software. Phylogenetic analysis
493 was carried out based on the neighbor-joining (NJ) method using MEGA10.1.8 software.
494
495 **qRT-PCR for mRNAs and miRNAs**
496 To examine the temporal expression profile of *CcTRPM*, summer-form samples were
497 collected at different developmental stages, including egg; nymphs of the 1st, 2nd, 3rd, 4th, and
498 5th instar; adults of 1, 5, and 10 days. For the effect of different temperatures treatment on the
499 mRNA expression of *CcTRPM*, miR-252, and chitin biosynthesis signaling genes, summer-form
500 1st instar nymphs were treated at 25°C and 10°C. Samples of nymphs were collected at 1, 2, 3, 6,
501 and 10 days after different temperatures treatment and immediately stored at -80°C. Each sample
502 was performed in three replications, with about 100 individuals for each replication of egg

503 samples and at least 50 insects were included for each nymph or adult samples. All samples were
504 immediately stored at -80°C for total RNA extraction.
505 Total RNA was isolated from the above samples using TRNzol Universal (Cat# DP424,
506 TIANGEN, Beijing, China) and miRcute miRNA isolation kit (Cat# DP501, TIANGEN, Beijing,
507 China) for mRNA and miRNA according to the manufacturer' instruction, respectively. The
508 first-strand cDNAs of mRNA and mature miRNA were synthesized from 500 ng of total RNA
509 using PrimeScript™ RT reagent kit with gDNA Eraser (Cat# RR047A, Takara, Kyoto, Japan) and
510 miRcute Plus miRNA First-Strand cDNA Synthesis Kit (Cat# KR211, TIANGEN, Beijing, China)
511 following the instruction manual. The relative expression of mRNA and miRNA was respectively
512 quantified using TB Green® *Premix Ex Taq*™ II (Tli RNaseH Plus) (Cat# RR820A, Takara, Kyoto,
513 Japan) and miRcute Plus miRNA qPCR Detection Kit (Cat# FP411, TIANGEN, Beijing, China)
514 in a 20 μL reaction mixture on a Bio-Rad CFX Connect™ Real-Time PCR System (Bio-Rad,
515 Hercules, CA, USA). To reduce the error, two reference genes of *C. chinensis*, *Ccβ-actin*
516 (GenBank accession number: OQ658571) and *CcEF-1* (GenBank accession number: OQ658572),
517 were used as internal controls for real-time PCR. U6 snRNA of *C. chinensis* was used as reference
518 gene for miRNA expression. To check for the specificity, melting curves were analyzed for each
519 data point (Figure S2, S6-S7). The specific reverse primer for miRNA expression was
520 complementary to the poly (T) adapter that was provided in the miRcute plus miRNA qPCR
521 detection kit. qRT-PCR data were quantified using the $2^{-\Delta\Delta CT}$ method, where ΔΔCT is equal to
522 $\Delta CT_{treated\ sample} - \Delta CT_{control}$ (Livak and Schmittgen, 2001).
523
524 **Ca^{2+} imaging and fluorescence detection of Fluo-4 AM**
525 The ORF sequence of *CcTRPM* was amplified by PCR with specific primers shown in Table
526 S1 and inserted into the pcDNA3.1(+)-mCherry vector to construct the recombinant vector of
527 CcTRPM-pcDNA3.1-mCherry using the *pEASY*®-Basic Seamless Cloning and Assembly Kit
528 (Cat# CU201, TransGen, Beijing, China). This recombinant vector was transfected into HEK293T
529 cells using TransIntro® EL Transfection Reagent (Cat# FT201, TransGen, Beijing, China) and the
530 cells were cultured for 20-40 h at 37°C. These transient-transfected cells were incubated in 500 μL
531 Fluo-4 AM (Cat# S1061, Beyotime, Shanghai, China) for 30 min at 37°C for staining and washed
532 for three times with Hank's Balanced Salt Solution. Then, these cells were treated with different
533 temperatures, different cooling agents, and used for Ca^{2+} imaging by a Leica SP8 confocal
534 microscopy (Weztlar, Germany) or for fluorescence detection of Fluo-4 AM by a Molecular
535 Devices i3x microplate reader (San Jose, USA).
536
537 **Fluorescence *in situ* hybridization (FISH)**
538 FISH experiment was carried out as previously described with minor adjustment (Kliot et al.,
539 2014). Briefly, 20 nymphs for each sample were immersed in Carnoy's fixative (glacial acetic acid:
540 ethanol: chloroform, 1: 3: 6, vol/vol/vol) inside eppendorf tubes for at least 48 h at room
541 temperature. The fixed samples were washed with 50% ethanol for three times and decolorized in
542 6% H_2O_2 in ethanol for 48 h at room temperature. Prehybridization was performed with three
543 times for 10 min per time using the hybridization buffer (20 mM Tris-HCl, pH 8.0; 0.9 M NaCl;
544 0.01% sodium dodecyl sulfate; 30% formamide) without the probe in the dark. The probe
545 sequences of *CcTRPM*-Cy3 and miR-252-FAM are listed in Table S1 and synthesized in
546 GenePharma (Shanghai, China). Hybridize samples for 12 h in the dark in hybridization buffer

547 containing 1 μM fluorescent probe. Combine two probes with different fluorescent dyes for the
548 co-localization. After washing three times with PBST, cell nuclei were stained with DAPI (1
549 μg/mL) for 15 min and rinsed with PBST for 15 min. At last, the samples were transferred to the
550 microscope slide, mounted in mounting medium using a cover slip, and viewed under a Leica SP8
551 confocal microscopy (Weztlar, Germany). The dsCcTRPM treated samples or no-probe samples
552 were used as negative controls for the specificity of probe signal.
553
554 **dsRNA synthesis and RNAi assay**
555 Double-stranded RNAs (dsRNAs) of *EGFP*, *CcTRPM*, and 14 transcripts of chitin
556 biosynthesis signaling genes were prepared in vitro using primers ligated with T7 RNA
557 polymerase promoter sequences (Table S1) using MEGAscript™ RNAi kit (AM1626, Ambion,
558 California, USA). dsRNAs were further purified with MEGAclear columns (Ambion) and eluted
559 with diethyl pyrocarbonate (DEPC)-treated nuclease-free water. The purity and concentration of
560 dsRNA were then measured via ultraviolet spectrophotometry and gel electrophoresis. The above
561 stem-leaf device was used for dsRNA feeding and RNAi assay.
562 For the RNAi assays, summer-form 1st instar nymphs were fed with different dsRNAs (500
563 ng/μL) and divided into three groups. (1) The samples were collected after dsRNAs feeding at 2 d
564 and 4 d under 25°C condition, and at 3 d and 6 d under 10°C condition, then for the RNAi
565 efficiency analysis and miR-252 expression by qRT-PCR. (2) Observed the morphological
566 characteristics every two days and counted the number of summer-form and winter-form
567 individuals based on the above description until the 3rd instar under 10°C condition. (3) The
568 samples were collected after dsRNA feeding at 12 d for cuticle ultrastructure comparison, cuticle
569 chitin staining with WGA-FITC, and determination of cuticle chitin content under 10°C condition
570 according to the above methods.
571 For the rescue by menthol feeding under dsCcTRPM treatment, summer-form 1st instar
572 nymphs were fed with the mixture of dsCcTRPM (500 ng/μL) and menthol (1 mg/mL), then
573 counted the number of summer-form and winter-form individuals following the above method
574 until the 3rd instar under 10°C condition. All the experiments were performed in three replications
575 with at least 30 nymphs for each replication.
576
577 **Prediction of miRNAs for *CcTRPM***
578 The 3'UTR sequence of *CcTRPM* gene was amplified by the 3'-Full RACE Core Set with
579 PrimeScript™ RTase kit (Cat# 6106, Takara, Kyoto, Japan). miRNAs for *CcTRPM* were
580 predicted by a service provider LC science with two software programs of miRanda
581 (http://www.microrna.org) and Targetscan (https://www.targetscan.org/vert_72/) with the default
582 parameters (Enright et al., 2003; Agarwal et al., 2015). For software miRanda, the alignment
583 scores of 145 and -15 kcal/mol were set to the threshold. The context score percentile of
584 Targetscan was set as larger than 50 to evaluate the target relationship between miRNA and
585 potential targets. The overlapped miRNAs predicted through both methods were selected.
586
587 ***In vitro* luciferase activity assay**
588 The 419 bp sequence of 3'UTR containing predicted target sites for miR-252 in *CcTRPM*
589 was cloned into the pmirGLO vector (Promega, Wisconsin, USA) downstream of the luciferase
590 gene to construct the recombinant plasmid of CcTRPM-3'UTR-pmirGLO using the *pEASY*®-Basic

591 Seamless Cloning and Assembly Kit. The mutated 3'UTR sequence was amplified and cloned into
592 the pmirGLO vector to generate the CcTRPM-3'UTR mutant-pmirGLO plasmid. The agomir and
593 antagomir of miRNAs were chemically synthesized and modified by GenePharma (Shanghai,
594 China) with chemically modified RNA oligos of the same sequence or anti-sense oligonucleotides
595 of the miRNA. The negative control for agomir and antagomir was provided by the manufacturer.
596 HEK293T cells were cultured in a 24-well plate at 37°C in 5% CO_2 overnight and transfected with
597 CcTRPM-3'UTR-pmirGLO plasmid (approximate 500 ng) or CcTRPM-3'UTR mutant-pmirGLO
598 plasmid (approximately 500 ng) and 275 nM agomir-miRNA or agomir-NC using the Calcium
599 Phosphate Cell Transfection Kit (Cat# C0508, Beyotime, Nanjing, China). The activity of the two
600 luciferase enzymes was measured 24 h after co-transfection following the manufacturer's
601 instruction of Dual-Luciferase® Reporter Assay System (Cat# E1910, Promega, Wisconsin, USA).
602 Nine biological replications were carried out for each transfection.
603
604 ***In vivo* RNA-binding protein immunoprecipitation Assay (RIP)**
605 A Magna RIP Kit (Cat# 17-704, Merck, Millipore, Germany) was used to perform the RIP
606 assay following the manufacturer's instruction. Specifically, approximately 50 summer-form 1st
607 instar nymphs were fed with agomir-252 or agomir-NC for 24 h. The treated nymphs were
608 collected and crushed with an auto homogenizer in ice-cold RIP lysis buffer, then stored at -80°C
609 overnight. Next, 50 μL magnetic beads were incubated with 5 μg of Ago-1 antibody (Merck,
610 Millipore, Germany) or IgG antibody (Merck, Millipore, Germany) to form bead-antibody
611 complex. The frozen lysates were thawed and centrifuged, and the supernatants were divided into
612 three equal parts. One part is considered as an "input" sample and stored at -80°C for qRT-PCR
613 analysis. The other two parts were incubated with the magnetic bead-antibody complex
614 (anti-Ago1 or IgG) at 4°C overnight. The immunoprecipitated RNAs were released by digestion
615 with protease K and extracted by the above methods. Finally, the abundance of *CcTRPM* and
616 miR-252 were quantified by qRT-PCR. The "input" samples and IgG controls were assayed to
617 normalize the relative expression of target genes and ensure the specificity of the RNA-protein
618 interactions. Six replications were carried out for each treatment.
619
620 **Feeding treatment of agomir-252 and antagomir-252**
621 To determine the effect of miR-252 on *CcTRPM* expression, summer-form 1st instar nymphs
622 were fed with agomir-252 (1 μM) or antagomir-252 (1 μM) and collected at 6 d after treatment for
623 qRT-PCR. Agomir/antagomir negative control was fed as the control. To test the effect of
624 miR-252 on the transition of summer-form to winter-form, summer-form 1st instar nymphs were
625 fed with agomir-252 (1 μM) or agomir-NC (1 μM) and divided into three groups. (1) The samples
626 were collected after different agomir feeding at 3 d and 6 d under 10°C condition, then for
627 miR-252 expression analysis using qRT-PCR. (2) The samples were collected after agomir
628 feeding at 12 d for cuticle ultrastructure comparison, cuticle chitin staining with WGA-FITC, and
629 determination of cuticle chitin content under 10°C condition according to the above methods. (3)
630 Observed the morphological characteristics every two days and counted the number of
631 summer-form and winter-form individuals based on the above description until the 3rd instar
632 under 10°C condition.
633 For the rescue by antagomir-252 feeding under dsCcTRPM treatment, summer-form 1st
634 instar nymphs were fed with the mixture of antagomir-252 (1 μM) and dsCcTRPM (500 ng/μL),

then counted the number of summer-form and winter-form individuals based the above method until the 3rd instar under 10°C condition. All the experiments were performed in nine replications with at least 30 nymphs for each replication.

Statistical analysis

GraphPad Prism 8.0 software and IBM SPSS Statistics 26.0 were used for making figures and statistical analysis, respectively. All the data were shown as means ± standard deviation (SD) with different independent biological replications. Student's *t*-test was performed for pairwise comparisons to determine the statistically significant differences between treatments and controls (***$P < 0.001$). One-way ANOVA followed by the Tukey's HSD multiple comparison test was used for multiple comparisons (different letters denoted by $P < 0.05$).

Acknowledgements

Thanks for the funding support by the National Natural Science Foundation of China (32202291), China Agriculture Research System (CARS-28), and Chinese Universities Scientific Fund (2023TC048).

Authors' contributions

S.Z., and X.L. designed research; S.Z., J.L., and D.Z. performed research; Z.Z., and S.M. contributed new analytic tools; S.Z., J.L., D.Z., Z.Z., S.M., and Z.L. analyzed data; S.Z. wrote the paper; and S.Z., and X.L. provided the fund.

Data accessibility

The published article includes all data generated or analyzed during this study. The full sequences were submitted to NCBI, accession number: OQ658558 for *CcTRPM*, OQ734934 for *CcTre1*, and OQ658570 for *CcCHS1*.

Funding

This work was funded by the National Natural Science Foundation of China (32202291), China Agriculture Research System (CARS-28), and Chinese Universities Scientific Fund (2023TC048).

Competing interests

The authors declared no competing financial interests.

669 **References**

670 Agarwal, V., Bell, G. W., Nam, J.W., & Bartel, D. P. (2015). Predicting effective microRNA
671 target sites in mammalian mRNAs. *ELife*, *4*, e05005. https://doi.org/10.7554/eLife.05005
672 An, C., Fei, X., Chen, W., & Zhao, Z. (2012). The integrative effects of population density,
673 photoperiod, temperature, and host plant on the induction of alate aphids in *Schizaphis*
674 *graminum*. *Archives of Insect Biochemistry and Physiology*, *79*(4–5), 198–206.
675 https://doi.org/10.1002/arch.21005
676 Asgari, S. (2013). MicroRNA functions in insects. *Insect Biochemistry and Molecular Biology*,
677 *43*(4), 388–397. https://doi.org/10.1016/j.ibmb.2012.10.005
678 Butt, B. A., & Stuart, C. (1986). Oviposition by summer and winter forms of *Pear Psylla*
679 (Homoptera: Psyllidae) on dormant pear budwood. *Environmental Entomology*, *5*,
680 1109–1110. https://doi.org/10.1093/ee/15.5.1109
681 Cao, E., Cordero-Morales, J. F., Liu, B. Y., Qin, F., Julius, D. (2013). TRPV1 channels are
682 intrinsically heat sensitive and negatively regulated by phosphoinositide lipids. *Neuron*,
683 77(4): 667–679. doi:10.1016/j.neuron.2012.12.016.
684 Caterina, M. J., Schumacher, M. A., Tominaga, M., Rosen, T. A., Levine, J. D., Julius, D. (1997).
685 The capsaicin receptor: a heat-activated ion channel in the pain pathway. *Nature*, 389,
686 816-824. DOI: 10.1126/science.288.5464.306
687 Chen, S., Nichols, K. M., Poynton, H. C., & Sepúlveda, M. S. (2016). MicroRNAs are involved in
688 cadmium tolerance in *Daphnia pulex*. *Aquatic Toxicology (Amsterdam, Netherlands)*, *175*,
689 241–248. https://doi.org/10.1016/j.aquatox.2016.03.023
690 Cridge, A. G., Leask, M. P., Duncan, E. J., & Dearden, P. K. (2015). What do studies of insect
691 polyphenisms tell us about nutritionally-triggered epigenomic changes and their
692 consequences? *Nutrients*, *7*(3), 1787–1797. https://doi.org/10.3390/nu7031787
693 Dai, T.M., Wang, Y.S., Liu, W.X., Lü, Z.C., & Wan, F.H. (2018). Thermal discrimination and
694 transgenerational temperature response in *Bemisia tabaci* Mediterranean (Hemiptera:
695 Aleyrodidae): putative involvement of the thermo-sensitive receptor *BtTRPA*.
696 *Environmental Entomology*, *47*(1), 204–209. https://doi.org/10.1093/ee/nvx202
697 Doucet, D., Retnakaran, A. (2012). Insect Chitin-Chapter Six: Metabolism, Genomics and Pest
698 Management. *Advances in insect physiology*, 43, 437-511.
699 https://doi.org/10.1016/B978-0-12-391500-9.00006-1
700 Ekino, T., Yoshiga, T., Takeuchi-Kaneko, Y., & Kanzaki, N. (2017). Transmission electron
701 microscopic observation of body cuticle structures of phoretic and parasitic stages of
702 Parasitaphelenchinae nematodes. *PloS One*, *12*(6), e0179465.
703 https://doi.org/10.1371/journal.pone.0179465
704 Enright, A. J., John, B., Gaul, U., Tuschl, T., Sander, C., & Marks, D. S. (2003). MicroRNA
705 targets in *Drosophila*. *Genome Biology*, *5*(1), R1. https://doi.org/10.1186/gb-2003-5-1-r1
706 Evans, A. R., & Sanson, G. D. (2005). Biomechanical properties of insects in relation to
707 insectivory: Cuticle thickness as an indicator of insect "hardness" and "intractability."
708 *Australian Journal of Zoology*, *53*(1), 9–19. https://doi.org/10.1071/zo04018
709 Farnesi, L. C., Brito, J. M., Linss, J. G., Pelajo-Machado, M., Valle, D., & Rezende, G. L. (2012).
710 Physiological and morphological aspects of *Aedes aegypti* developing larvae: effects of

the chitin synthesis inhibitor novaluron. *PLoS ONE*, *7*(1), e30363. https://doi.org/10.1371/journal.pone.0030363

Fedorka, K. M., Copeland, E. K., & Winterhalter, W. E. (2013). Seasonality influences cuticle melanization and immune defense in a cricket: support for a temperature-dependent immune investment hypothesis in insects. *The Journal of Experimental Biology*, *216*(Pt 21), 4005–4010. https://doi.org/10.1242/jeb.091538

Fu, T., Hull, J. J., Yang, T., & Wang, G. (2016). Identification and functional characterization of four transient receptor potential ankyrin 1 variants in *Apolygus lucorum* (Meyer-Dür). *Insect Molecular Biology*, *25*(4), 370–384. https://doi.org/10.1111/imb.12231

Ge, Y., Zhang, L., Qin, Z., Wang, Y., Liu, P., Tan, S., Fu, Z., Smith, O. M., & Shi, W. (2019). Different predation capacities and mechanisms of *Harmonia axyridis* (Coleoptera: Coccinellidae) on two morphotypes of pear psylla *Cacopsylla chinensis* (Hemiptera: Psyllidae). *PLoS ONE*, *14*(4), e0215834. https://doi.org/10.1371/journal.pone.0215834

Guo, S., Tian, Z., Wu, Q.W., King-Jones, K., Liu, W., Zhu, F., & Wang, X.P. (2021). Steroid hormone ecdysone deficiency stimulates preparation for photoperiodic reproductive diapause. *PLoS Genetics*, *17*(2), e1009352. https://doi.org/10.1371/journal.pgen.1009352

Hildebrand, M., Dickler, E., & Geider, K. (2010). Occurrence of *Erwinia amylovora* on insects in a fire blight orchard. *Journal of Phytopathology*, *148*(4), 251–256. https://doi.org/10.1046/j.1439-0434.2000.00504.x

Hou, L., Yang, P., Jiang, F., Liu, Q., Wang, X., & Kang, L. (2017). The neuropeptide F/nitric oxide pathway is essential for shaping locomotor plasticity underlying locust phase transition. *ELife*, *6*, e22526. https://doi.org/10.7554/eLife.22526

Kennell, J. A., Cadigan, K. M., Shakhmantsir, I., & Waldron, E. J. (2012). The microRNA miR-8 is a positive regulator of pigmentation and eclosion in *Drosophila*. *Developmental Dynamics: An Official Publication of the American Association of Anatomists*, *241*(1), 161–168. https://doi.org/10.1002/dvdy.23705

Kliot, A., Kontsedalov, S., Lebedev, G., Brumin, M., Cathrin, P. B., Marubayashi, J. M., Skaljac, M., Belausov, E., Czosnek, H., & Ghanim, M. (2014). Fluorescence in situ hybridizations (FISH) for the localization of viruses and endosymbiotic bacteria in plant and insect tissues. *Journal of Visualized Experiments: JoVE*, *84*, 51030. https://doi.org/10.3791/51030

Kreß, A., Kuch, U., Oehlmann, J., & Müller, R. (2016). Effects of diapause and cold acclimation on egg ultrastructure: new insights into the cold hardiness mechanisms of the Asian tiger mosquito *Aedes (Stegomyia) albopictus*. *Journal of Vector Ecology: Journal of the Society for Vector Ecology*, *41*(1), 142–150. https://doi.org/10.1111/jvec.12206

Lee, Y., Lee, Y., Lee, J., Bang, S., Hyun, S., Kang, J., Hong, S.T., Bae, E., Kaang, B.K., & Kim, J. (2005). Pyrexia is a new thermal transient receptor potential channel endowing tolerance to high temperatures in *Drosophila melanogaster*. *Nature Genetics*, *37*(3), 305–310. https://doi.org/10.1038/ng1513

Liu, F., Peng, W., Li, Z., Li, W., Li, L., Pan, J., Zhang, S., Miao, Y., Chen, S., & Su, S. (2012). Next-generation small RNA sequencing for microRNAs profiling in *Apis mellifera*: Comparison between nurses and foragers. *Insect Molecular Biology*, *21*(3), 297–303. https://doi.org/10.1111/j.1365-2583.2012.01135.x

754 Livak, K. J., & Schmittgen, T. D. (2001). Analysis of relative gene expression data using real-time
755 quantitative PCR and the $2^{-\Delta\Delta CT}$ method. *Methods*, *25*(4), 402–408.
756 https://doi.org/10.1006/meth.2001.1262
757 Lyons, P. J., Crapoulet, N., Storey, K. B., & Morin, P. (2015). Identification and profiling of
758 miRNAs in the freeze-avoiding gall moth *Epiblema scudderiana* via next-generation
759 sequencing. *Molecular and Cellular Biochemistry*, *410*(1–2), 155–163.
760 https://doi.org/10.1007/s11010-015-2547-3
761 Ma, Z., Guo, W., Guo, X., Wang, X., & Kang, L. (2011). Modulation of behavioral phase changes
762 of the migratory locust by the catecholamine metabolic pathway. *Proceedings of the*
763 *National Academy of Sciences of the United States of America*, *108*(10), 3882–3887.
764 https://doi.org/10.1073/pnas.1015098108
765 McKemy, D. D., Neuhausser, W. M., & Julius, D. (2002). Identification of a cold receptor reveals
766 a general role for TRP channels in thermosensation. *Nature*, *416*(6876), 52–58.
767 https://doi.org/10.1038/nature719
768 Minke, B., Wu, C., & Pak, W. L. (1975). Induction of photoreceptor voltage noise in the dark in
769 *Drosophila* mutant. *Nature*, *258*(5530), 84–87. https://doi.org/10.1038/258084a0
770 Morin, M. D., Frigault, J. J., Lyons, P. J., Crapoulet, N., Boquel, S., Storey, K. B., & Morin, P. J.
771 (2017). Amplification and quantification of cold-associated microRNAs in the Colorado
772 potato beetle (*Leptinotarsa decemlineata*) agricultural pest. *Insect Molecular Biology*,
773 *26*(5), 574–583. https://doi.org/10.1111/imb.12320
774 Neely, G. G., Keene, A. C., Duchek, P., Chang, E. C., Wang, Q.P., Aksoy, Y. A., Rosenzweig, M.,
775 Costigan, M., Woolf, C. J., Garrity, P. A., & Penninger, J. M. (2011). TrpA1 regulates
776 thermal nociception in *Drosophila*. *PloS One*, *6*(8), e24343.
777 https://doi.org/10.1371/journal.pone.0024343
778 Oldfield, & G., N. (1970). Diapause and polymorphism in california populations of *Psylla*
779 *pyricola* (Homoptera: Psyllidae). *Annals of the Entomological Society of America*, *63*(1),
780 180–184. https://doi.org/10.1093/aesa/63.1.180
781 Peier, A. M., Moqrich, A., Hergarden, A. C., Reeve, A. J., Andersson, D. A., Story, G. M., Earley,
782 T. J., Dragoni, I., McIntyre, P., Bevan, S., & Patapoutian, A. (2002). A TRP channel that
783 senses cold stimuli and menthol. *Cell*, *108*(5), 705–715.
784 https://doi.org/10.1016/S0092-8674(02)00652-9
785 Richards, A. G. (1978). The chemistry of insect cuticle. *Biochemistry of Insects*, 205–232.
786 https://doi.org/10.1016/B978-0-12-591640-0.50010-8
787 Rosenzweig, M., Kang, K., & Garrity, P. A. (2008). Distinct TRP channels are required for warm
788 and cool avoidance in *Drosophila melanogaster*. *Proceedings of the National Academy of*
789 *Sciences of the United States of America*, *105*(38), 14668–14673.
790 https://doi.org/10.1073/pnas.0805041105
791 Sato, A., Sokabe, T., Kashio, M., Yasukochi, Y., Tominaga, M., & Shiomi, K. (2014). Embryonic
792 thermosensitive TRPA1 determines transgenerational diapause phenotype of the
793 silkworm, *Bombyx mori*. *Proceedings of the National Academy of Sciences of the United*
794 *States of America*, *111*(13), E1249–E1255. https://doi.org/10.1073/pnas.1322134111
795 Shang, F., Niu, J., Ding, B.Y., Zhang, W., Wei, D.D., Wei, D., Jiang, H.B., & Wang, J.J. (2020).
796 The miR-9b microRNA mediates dimorphism and development of wing in aphids.

Proceedings of the National Academy of Sciences, *117*(15), 8404–8409. https://doi.org/10.1073/pnas.1919204117

Shiels, A. (2020). TRPM3_miR-204: A complex locus for eye development and disease. *Human Genomics*, *14*(1), 7. https://doi.org/10.1186/s40246-020-00258-4

Simpson, S. J., Sword, G. A., & Lo, N. (2011). Polyphenism in insects. *Current Biology*, *21*(18), R738–R749. https://doi.org/10.1016/j.cub.2011.06.006

Teets, N. M., Marshall, K. E., & Reynolds, J. A. (2023). Molecular mechanisms of winter survival. *Annual Review of Entomology*, *68*, 319–339. https://doi.org/10.1146/annurev-ento-120120-095233

Terblanche, J. S., Hoffmann, A. A., Mitchell, K. A., Rako, L., le Roux, P. C., & Chown, S. L. (2011). Ecologically relevant measures of tolerance to potentially lethal temperatures. *The Journal of Experimental Biology*, *214*(Pt 22), 3713–3725. https://doi.org/10.1242/jeb.061283

Tougeron, K., Iltis, C., Renoz, F., Albittar, L., Hance, T., Demeter, S., & Le Goff, G. J. (2021). Ecology and biology of the parasitoid *Trechnites insidiosus* and its potential for biological control of pear psyllids. *Pest Management Science*, *77*(11), 4836–4847. https://doi.org/10.1002/ps.6517

Tracey, W. D., Wilson, R. I., Laurent, G., & Benzer, S. (2003). Painless, a *Drosophila* gene essential for nociception. *Cell*, *113*(2), 261–273. https://doi.org/10.1016/s0092-8674(03)00272-1

Tsuchiya, R., Kaneshima, A., Kobayashi, M., Yamazaki, M., Takasu, Y., Sezutsu, H., Tanaka, Y., Mizoguchi, A., & Shiomi, K. (2021). Maternal GABAergic and GnRH/corazonin pathway modulates egg diapause phenotype of the silkworm Bombyx mori. *Proceedings of the National Academy of Sciences of the United States of America*, *118*(1), e2020028118. https://doi.org/10.1073/pnas.2020028118

Turner, H. N., Armengol, K., Patel, A. A., Himmel, N. J., Sullivan, L., Iyer, S. C., Bhattacharya, S., Iyer, E. P. R., Landry, C., Galko, M. J., & Cox, D. N. (2016). The TRP channels Pkd2, NompC and Trpm act in cold-sensing neurons to mediate unique aversive behaviors to noxious cold in Drosophila. *Current Biology: CB*, *26*(23), 3116–3128. https://doi.org/10.1016/j.cub.2016.09.038

Vargas, H. C. M., Farnesi, L. C., Martins, A. J., Valle, D., & Rezende, G. L. (2014). Serosal cuticle formation and distinct degrees of desiccation resistance in embryos of the mosquito vectors Aedes aegypti, Anopheles aquasalis and Culex quinquefasciatus. *Journal of Insect Physiology*, *62*, 54–60. https://doi.org/10.1016/j.jinsphys.2014.02.001

Vellichirammal, N. N., Gupta, P., Hall, T. A., & Brisson, J. A. (2017). Ecdysone signaling underlies the pea aphid transgenerational wing polyphenism. *Proceedings of the National Academy of Sciences of the United States of America*, *114*(6), 1419–1423. https://doi.org/10.1073/pnas.1617640114

Venkatachalam, K., & Montell, C. (2007). TRP channels. *Annual Review of Biochemistry*, *76*, 387–417. https://doi.org/10.1146/annurev.biochem.75.103004.142819

Wang, L.-X., Niu, C.-D., Wu, S.-F., & Gao, C.-F. (2021). Molecular characterizations and expression profiles of transient receptor potential channels in the brown planthopper, Nilaparvata lugens. *Pesticide Biochemistry and Physiology*, *173*, 104780. https://doi.org/10.1016/j.pestbp.2021.104780

Wang, X.-D., Lin, Z.-K., Ji, S.-X., Bi, S.-Y., Liu, W.-X., Zhang, G.-F., Wan, F.-H., & Lü, Z.-C. (2021). Molecular characterization of TRPA subfamily genes and function in temperature preference in *Tuta absoluta* (Meyrick) (Lepidoptera: Gelechiidae). *International Journal of Molecular Sciences*, *22*(13), 7157. https://doi.org/10.3390/ijms22137157

Wei, M., Chi, H., Guo, Y., Li, X., Zhao, L., & Ma, R. (2020). Demography of *Cacopsylla chinensis* (Hemiptera: Psyllidae) reared on four cultivars of *Pyrus bretschneideri* (Rosales: Rosaceae) and *P. communis* Pears with estimations of confidence intervals of specific life table statistics. *Journal of Economic Entomology*, *113*(5), 2343–2353. https://doi.org/10.1093/jee/toaa149

Xie, J., Peng, G., Wang, M., Zhong, Q., Song, X., Bi, J., Tang, J., Feng, F., Gao, H., & Li, B. (2022). RR-1 cuticular protein TcCPR69 is required for growth and metamorphosis in *Tribolium castaneum*. *Insect Science*, *29*(6), 1612–1628. https://doi.org/10.1111/1744-7917.13038

Xu, H.J., Xue, J., Lu, B., Zhang, X.C., Zhuo, J.C., He, S.F., Ma, X.F., Jiang, Y.Q., Fan, H.W., Xu, J.Y., Ye, Y.X., Pan, P.L., Li, Q., Bao, Y.Y., Nijhout, H. F., & Zhang, C.X. (2015). Two insulin receptors determine alternative wing morphs in planthoppers. *Nature*, *519*(7544), 464–467. https://doi.org/10.1038/nature14286

Yang, M., Wei, Y., Jiang, F., Wang, Y., Guo, X., He, J., & Kang, L. (2014). MicroRNA-133 inhibits behavioral aggregation by controlling dopamine synthesis in Locusts. *PLoS Genetics*, *10*(2), e1004206. https://doi.org/10.1371/journal.pgen.1004206

Yang, S., Zhang, J., Wang, S., Zhang, X., Liu, Y., & Xi, J. (2017). Identification and profiling of miRNAs in overwintering *Lissorhoptrus oryzophilus* via next-generation sequencing. *Cryobiology*, *74*, 68–76. https://doi.org/10.1016/j.cryobiol.2016.11.013

Yang, X., Wu, D., Du, H., Nie, F., Pang, X., & Xu, Y. (2017). MicroRNA-135a is involved in podocyte injury in a transient receptor potential channel 1-dependent manner. *International Journal of Molecular Medicine*, *40*(5), 1511–1519. https://doi.org/10.3892/ijmm.2017.3152

Ye, X., Xu, L., Li, X., He, K., Hua, H., Cao, Z., Xu, J., Ye, W., Zhang, J., Yuan, Z., & Li, F. (2019). MiR-34 modulates wing polyphenism in planthopper. *PLoS Genetics*, *15*(6), e1008235. https://doi.org/10.1371/journal.pgen.1008235

Zhang, B., Zhao, L., Ning, J., Wickham, J. D., Tian, H., Zhang, X., Yang, M., Wang, X., & Sun, J. (2020). MiR-31-5p regulates cold acclimation of the wood-boring beetle *Monochamus alternatus* via ascaroside signaling. *BMC Biology*, *18*(1), 184. https://doi.org/10.1186/s12915-020-00926-w

Zhang, J.L., Chen, S.J., Liu, X.Y., Moczek, A. P., & Xu, H.J. (2022). The transcription factor Zfh1 acts as a wing-morph switch in planthoppers. *Nature Communications*, *13*(1), 5670. https://doi.org/10.1038/s41467-022-33422-6

879 **Figure legends**

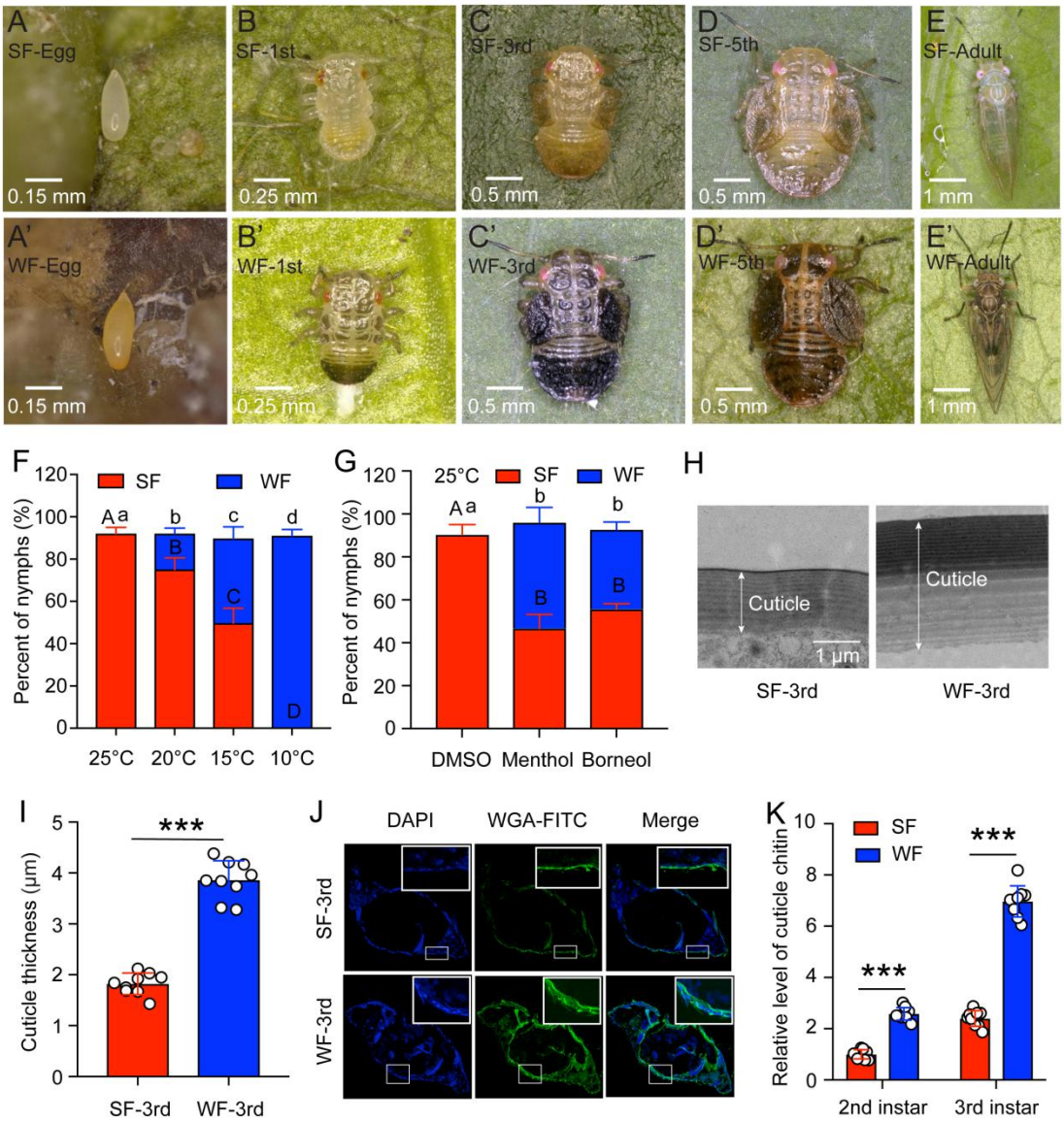

880

881 **Figure 1. Low temperature induced the transition from summer form (SF) to winter form**
882 **(WF) in *C. chinensis*.**

883 A-E and A'-E': The morphology of egg, 1st, 3rd, and 5th instar nymph, 5 days adult for SF and
884 WF of *C. chinensis*, respectively. The scale bars were labeled in the lower left of each figure.

885 F: Percent of SF and WF under different temperatures (25°C, 20°C, 15°C, and 10°C) when
886 induction of newly-hatched (within 12 h) 1st instar nymph of *C. chinensis*.

887 G: Effect of two chemical cooling agents (menthol and borneol) on the percent of SF and WF
888 when induction of newly-hatched (within 12 h) 1st instar nymph of *C. chinensis* under 25°C.

889 H: Ultrastructure comparison of the nymph cuticle for SF 3rd instar and WF 3rd instar of *C.*
890 *chinensis* using transmission electron microscopy. Scale bar is 1 μm. The two-way arrow
891 indicated the cuticle thickness.

892 I: Comparison of the nymph cuticle thickness for SF 3rd instar and WF 3rd instar of *C. chinensis*.

893 J: Chitin staining of nymph cuticle with WGA-FITC in SF 3rd instar and WF 3rd instar of *C.*

894 *chinensis*. DAPI: the cell nuclei were stained with DAPI and visualized in blue. WAG-FITC: the
895 cuticle chitin was labeled with FITC and visualized in green. Merge: merged imaging of DAPI,
896 and WAG-FITC signals.
897 K: Determination of cuticle chitin content in 2nd and 3rd instar nymph of SF and WF.
898 The data of nymph percent were shown as the mean ± SD with three independent biological
899 replications of at least 30 nymphs for each biological replication. Different letters above the bars
900 indicated statistically significant differences ($p < 0.05$), as determined by ANOVA followed with
901 a Turkey's HSD multiple comparison test in SPSS 20.0 software. The results of cuticle thickness
902 and cuticle chitin content were presented as mean ± SD of three independent biological samples
903 with three technical replications for each biological replication. Statistically significant differences
904 were determined with the pair-wise Student's *t*-test, and significance levels were denoted by *** (p
905 < 0.001).
906

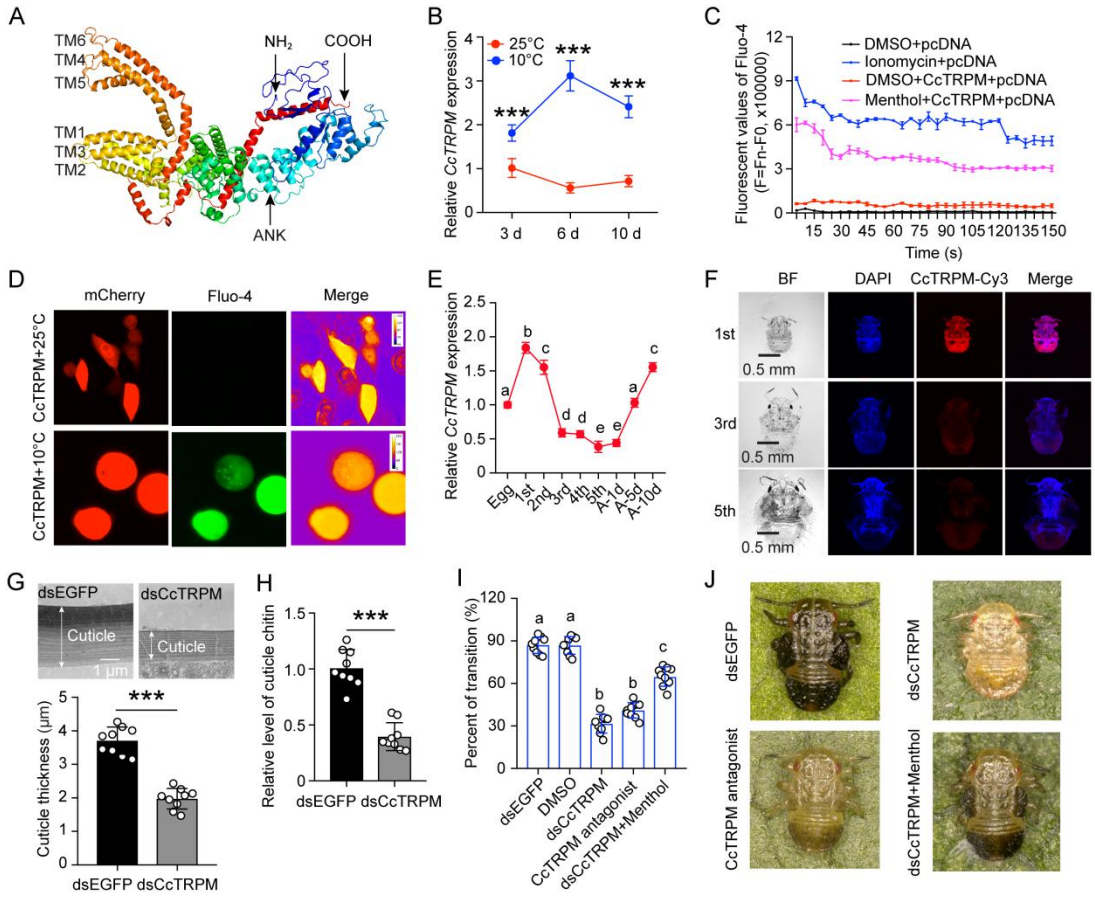

907
908 **Figure 2. Temperature receptor *CcTRPM* modulated the transition from SF to WF of *C.***
909 ***chinensis* in response to low temperature.**
910 A: The predicted protein tertiary structure of *CcTRPM*. The conserved ankyrin repeat (ANK)
911 domain was indicated in the N-terminal. The conserved six transmembrane domain of ion
912 channels structure were shown as TM1-TM6.
913 B: The mRNA expression of *CcTRPM* in response to different temperatures of 25°C and 10°C by
914 qRT-PCR.
915 C: Fluorescence detection of Fluo-4 AM after heterologous expression of *CcTRPM* in mammalian
916 HEK293T cells in response to menthol treatment. The recombinant plasmid was generated by

917 inserting the full ORF sequence of *CcTRPM* into pcDNA3.1(+)-mCherry plasmid. DMSO
918 treatment and ionomycin treatment were used as negative control and positive control, separately.
919 D: Representative images of Ca^{2+} imaging after heterologous expression of *CcTRPM* in
920 mammalian HEK293T cells in response to different temperature treatment. "CcTRPM+10°C"
921 means the recombinant plasmid of *CcTRPM* with pcDNA3.1(+)-mCherry was treated with 10°C.
922 "CcTRPM+25°C" denotes the pcDNA3.1(+)-mCherry plasmid with *CcTRPM* was treated with
923 25°C. mCherry and Fluo-4 signal are shown in red and green, respectively.
924 E: The developmental expression pattern of *CcTRPM* for SF at mRNA level using qRT-PCR. 1st,
925 2nd, 3rd, 4th and 5th are the nymphs at the first, second, third, fourth and fifth instar, respectively.
926 A-1d, A-5d, and A-10d are the adults at 1 day, 5 days, and 10 days, separately.
927 F: Representative confocal images of *CcTRPM* in different developmental stages of SF using
928 FISH. Scale bar is 0.5 mm. BF: the bright field. DAPI: the cell nuclei were stained with DAPI and
929 visualized in blue. CcTRPM-Cy3: CcTRPM signal was labeled with Cy3 and visualized in red.
930 Merge: merged imaging of BF, DAPI, and CcTRPM-Cy3 signals.
931 G-H: Comparison of the nymph cuticle ultrastructure, cuticle thickness, and cuticle chitin content
932 of SF 1st instar treated with dsCcTRPM and dsEGFP at 15 d.
933 I: The transition percent of SF 1st instar nymphs treated with dsEGFP, DMSO, dsCcTRPM,
934 CcTRPM antagonist and dsCcTRPM+menthol at 15 d under 10°C. For RNAi experiments,
935 summer-form 1st instar nymphs were fed with dsEGFP (500 ng/μL) or dsCcTRPM (500 ng/μL).
936 To mimic RNAi effect, summer-form 1st instar nymphs were fed with 0.1% DMSO or CcTRPM
937 antagonist (20 ng/μL). For the rescue experiment, summer-form 1st instar nymphs were fed with
938 the mixture of dsCcTRPM (500 ng/μL) and menthol (1 mg/mL). Then, counted the number of
939 summer-form and winter-form individuals and calculated the transition percent.
940 J: The phenotypes of SF 1st instar nymphs treated with dsEGFP, dsCcTRPM, CcTRPM antagonist
941 and dsCcTRPM+menthol at 15 d under 10°C.
942 The data in 2B and 2E are shown as the mean ± SD with three independent biological replications
943 of at least 30 nymphs for each biological replication. Data in 2G and 2H are presented as mean ±
944 SD with three biological replications of three technical replicates for each biological replication.
945 Data in 2I are presented as mean ± SD with nine biological replications. Statistically significant
946 differences were determined with the pair-wise Student's *t*-test, and significance levels were
947 denoted by *** ($p < 0.001$). Different letters above the bars indicated statistically significant
948 differences ($p < 0.05$), as determined by ANOVA followed with a Turkey's HSD multiple
949 comparison test in SPSS 20.0 software.
950

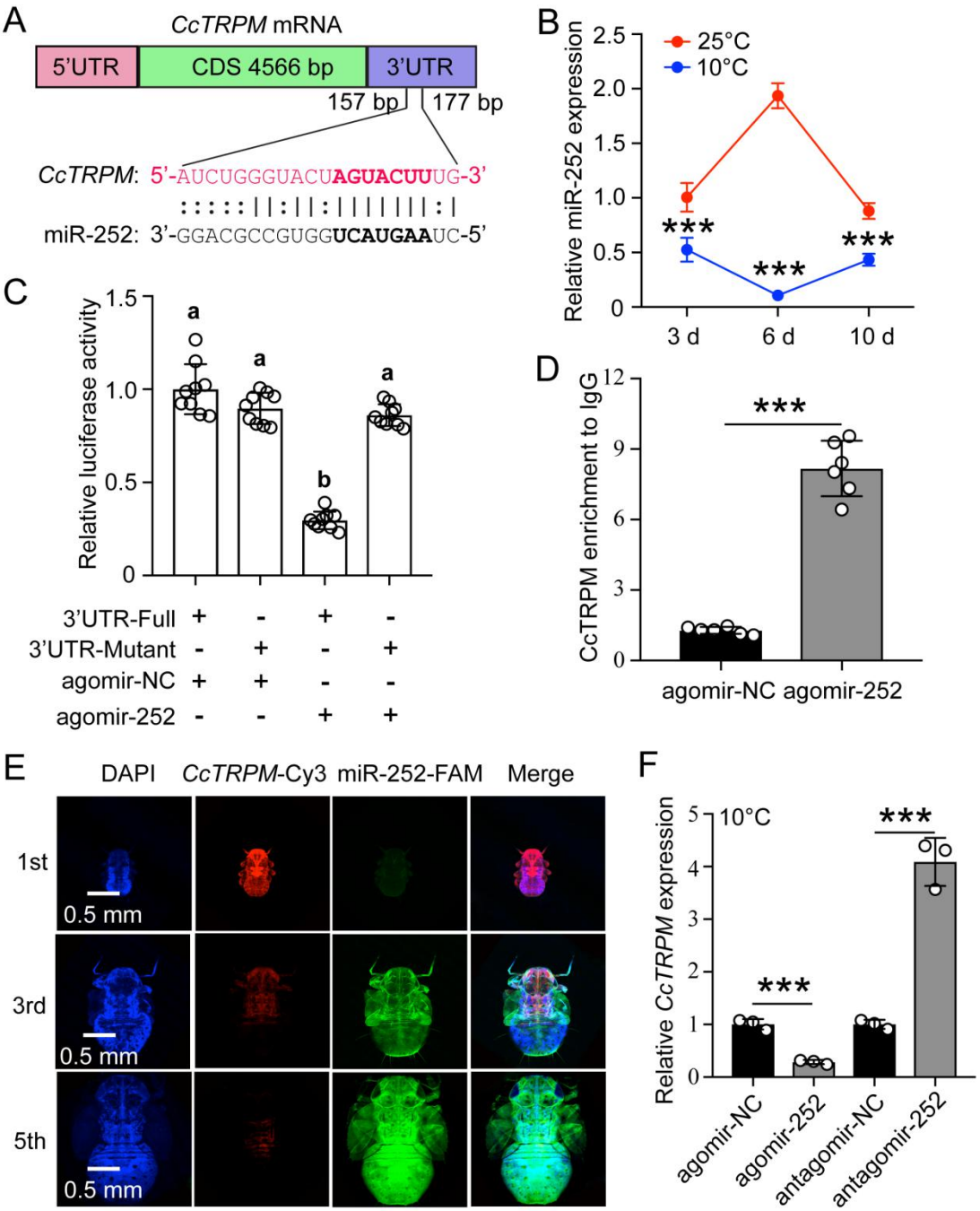

Figure 3. Confirming of miR-252 targeted *CcTRPM*.

A: The putative miR-252 binding sites in *CcTRPM* 3'UTR were predicted by miRanda and Targetscan.

B: The expression profiles of miR-252 in response to different temperatures of 25°C and 10°C by qRT-PCR.

C: In vitro validation of the target interactions between miR-252 and *CcTRPM* by dual luciferase reporter assays.

D: In vivo demonstration of miR-252 targeting *CcTRPM* by RNA-binding protein immunoprecipitation (RIP) assay.

E: Representative confocal images of miR-252 and *CcTRPM* in 1st, 3rd and 5th instar of SF. Scale bar is 0.5 mm. The signals of DAPI and *CcTRPM*-Cy3 are same as the above describing.

963 miR-252-FAM: the miR-252 signal was labeled with FAM and visualized in green. Merge:
964 merged imaging of co-localization of cell nucleus, *CcTRPM* and miR-252.
965 F: Effect of miR-252 agomir and antagomir treatment 3 days on the expression of *CcTRPM* at
966 mRNA level.
967 The data in 3B and 3F are shown as the mean ± SD with three independent biological replications
968 of at least 30 nymphs for each biological replication. Data in 3C are presented as mean ± SD with
969 nine biological replications. Data in 3D are presented as mean ± SD with two biological
970 replications of three technical replicates for each biological replication. Statistically significant
971 differences were determined with the pair-wise Student's *t*-test, and significance levels were
972 denoted by *** ($p < 0.001$). Different letters above the bars indicated statistically significant
973 differences ($p < 0.05$), as determined by ANOVA followed with a Turkey's HSD multiple
974 comparison test in SPSS 20.0 software.
975

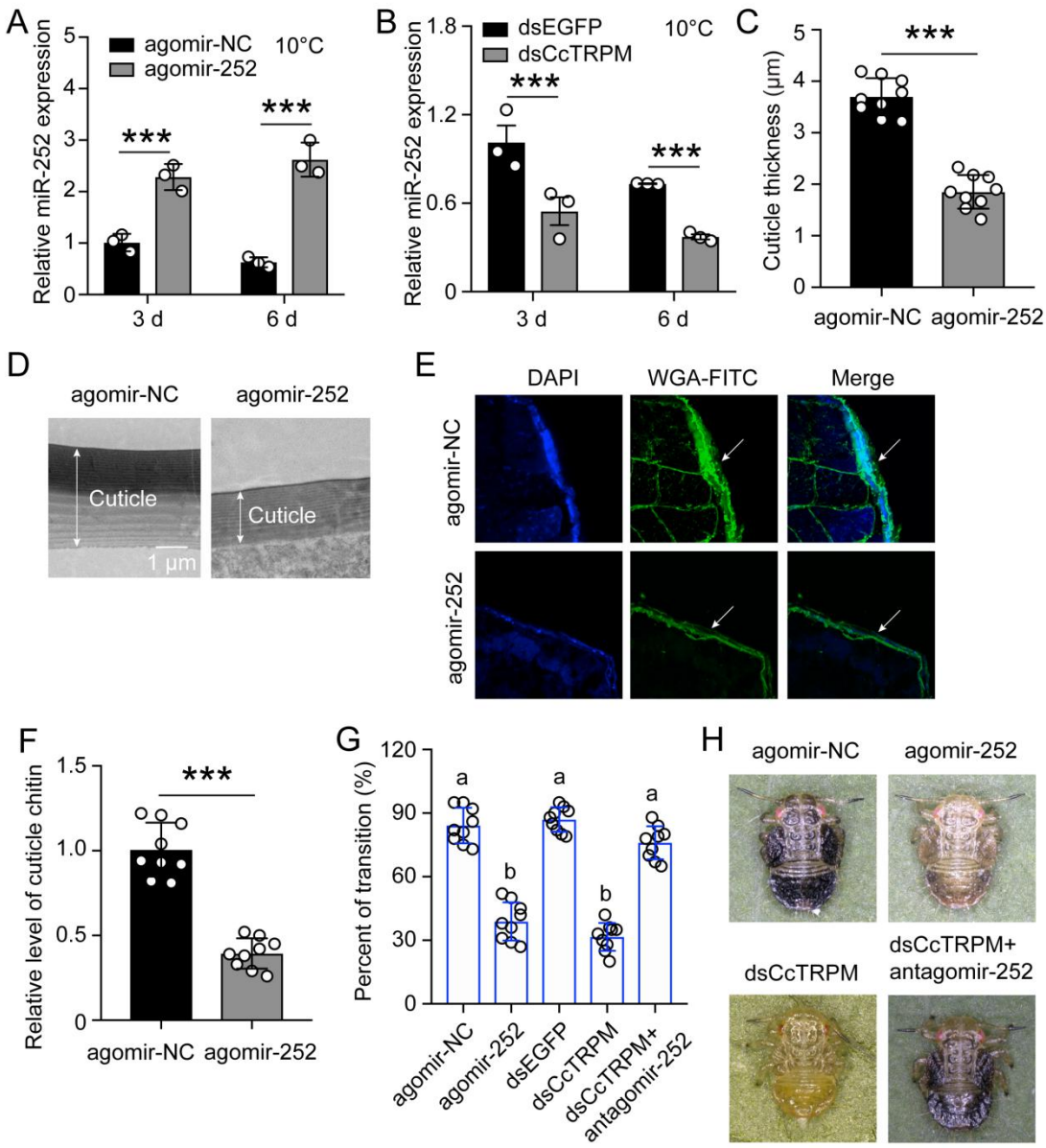

976
977 **Figure 4. miR-252 mediated the transition from SF to WF in *C. chinensis* by suppressing**

978 ***CcTRPM.***
979 A: Effect of miR-252 agomir treatment on the mRNA expression of miR-252 after 3 d and 6 d
980 under 10°C. agomir-NC treatment was used as the control. 3 d: 3 days. 6 d: 6 days.
981 B: The mRNA expression of miR-252 after dsCcTRPM treatment 3 d and 6 d compare with the
982 dsEGFP treatment under 10°C.
983 C-F: Comparison of the nymph cuticle thickness, cuticle ultrastructure, cuticle chitin staining with
984 WGA-FITC, and chitin content of SF 1st instar after treatment with agomir-NC and agomir-252 at
985 15 d. Scale bar is 1 μm. The two-way arrow indicated the cuticle thickness. The DAPI and
986 WAG-FITC signals were same as the above describing.
987 G: The transition percent of SF 1st instar nymphs treated with agomir-NC, agomir-252, dsEGFP,
988 dsCcTRPM, and dsCcTRPM+antagomir-252 at 15 d under 10°C.
989 H: The phenotypes of SF 1st instar nymphs treated with agomir-NC, agomir-252, dsCcTRPM, and
990 dsCcTRPM+antagomir-252 at 15 d under 10°C.
991 The data in 4A and 4B are shown as the mean ± SD with three independent biological replications
992 of at least 30 nymphs for each biological replication. Data in 4C and 4F are presented as mean ±
993 SD with three biological replications of three technical replications for each biological replication.
994 Data in 4G are presented as mean ± SD with nine biological replications. Statistically significant
995 differences were determined with the pair-wise Student's *t*-test, and significance levels were
996 denoted by *** ($p < 0.001$). Different letters above the bars indicated statistically significant
997 differences ($p < 0.05$), as determined by ANOVA followed with a Turkey's HSD multiple
998 comparison test in SPSS 20.0 software.
999

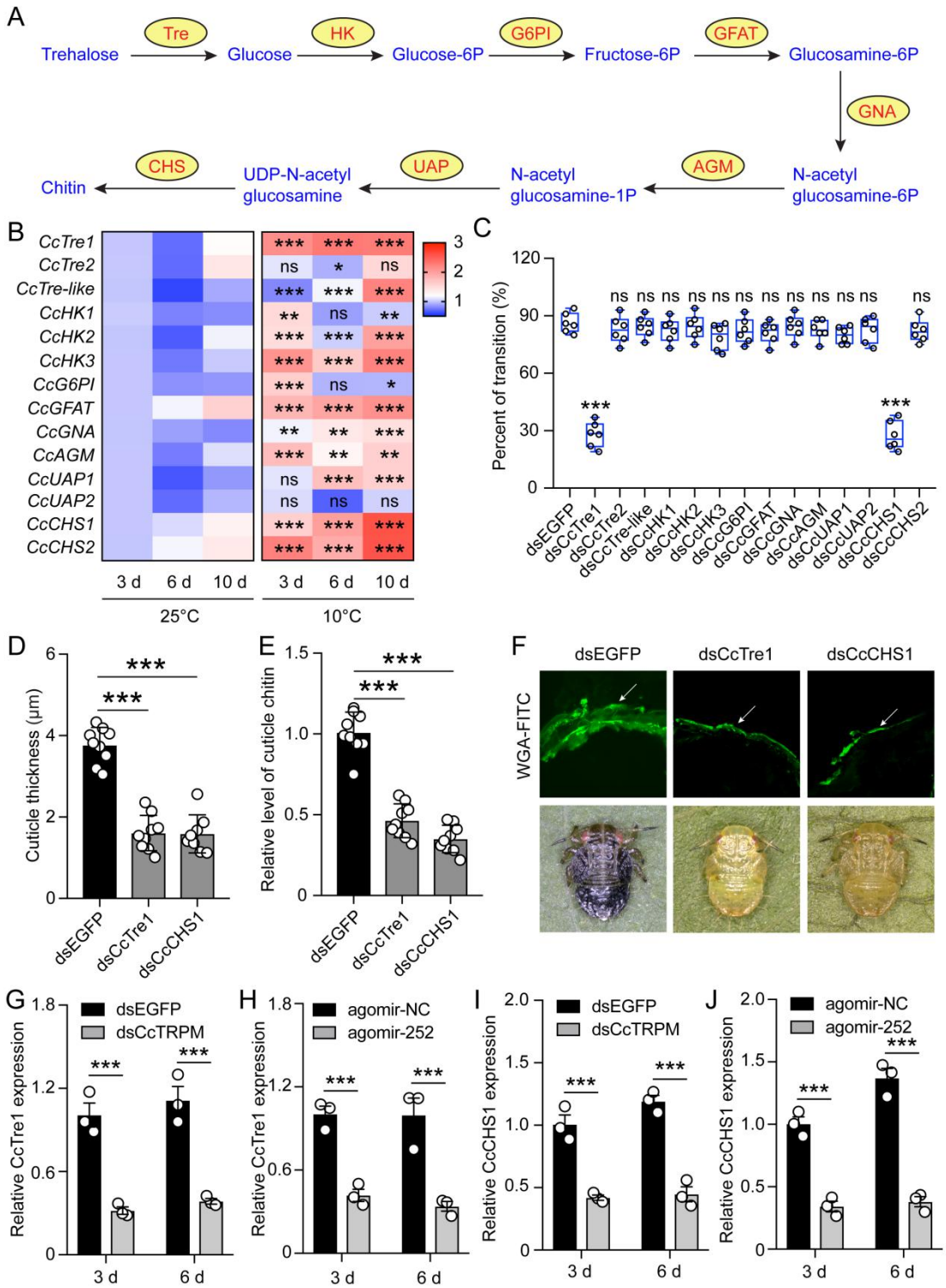

Figure 5. Chitin biosynthesis signaling involved in the transition from SF to WF of *C. chinensis* in response to low temperature and *CcTRPM*.

A: Diagram of de novo biosynthesis of insect chitin. Tre: trehalase. HK: hexokinase. G6PI: glucose-6-phosphate isomerase. GFAT: fructose-6-phosphate aminotransferase. GNA: glucosamine-6-phosphate acetyltransferase. AGM: N-acetylglucosamine phosphate mutase. UAP: UDP- N-acetylglucosamine pyrophosphorylase. CHS: chitin synthase.

B: A heat map was constructed from the expression levels of chitin biosynthesis enzyme

transcripts in *C. chinensis* after 25°C and 10°C treatment at 3 d, 6 d, and 10 d.

C: Effect of RNAi knockdown of 14 transcripts covering all the enzymes in the chitin biosynthesis pathway on the transition percent of SF 1st instar nymphs under 10°C.

D-F: Comparison of the nymph cuticle thickness, cuticle chitin content, and cuticle chitin staining with WGA-FITC of SF 1st instar after treatment with dsEGFP, dsCcTre1, and dsCcCHS1 at 15 d. The WAG-FITC signal was same as the above describing.

G-H: Effect of dsCcTRPM and agomir-252 treatments on the mRNA expression of *CcTre1* at 3 d and 6 d under 10°C.

I-J: Effect of dsCcTRPM and agomir-252 treatments on the mRNA expression of *CcCHS1* at 3 d and 6 d under 10°C.

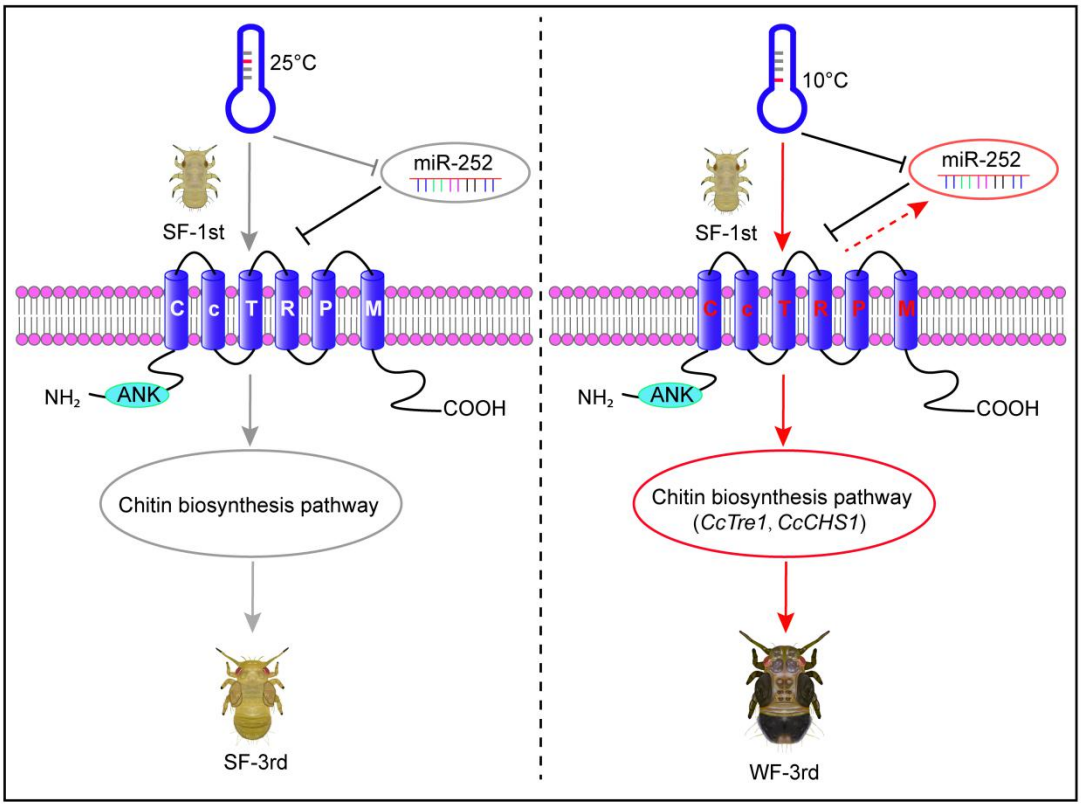

Figure 6. A model showing the key roles of miR-252 targeting *CcTRPM* to regulate the transition from SF to WF of *C. chinensis* in response to low temperature.

Under 25°C condition, the temperature receptor *CcTRPM* was inactive as inhibiting by miR-252 in 1st instar nymphs of SF. The 1st instar nymphs of SF normally developed into 3rd instar nymphs of SF. However, under 10°C condition, low temperature profoundly activated *CcTRPM* expression, miR-252 functioned as a negative regulator to mediate the expression of *CcTRPM* in case of over-expression in response to low temperature. Then, *CcTRPM* significantly increased the activity of chitin biosynthesis pathway, especially *CcTre1* and *CcCHS1*, and led to cuticle chitin content was obvious raise and cuticle thickness became thicker. Finally, the 1st instar nymphs of SF developed to 3rd instar nymphs of WF in order to better adapt to low temperature. Red arrows and black T-bars indicated the activation and inhibition, respectively. Gray arrows and T-bars represented the inactive states of the genes or physiological processes, separately.

Supplemental information

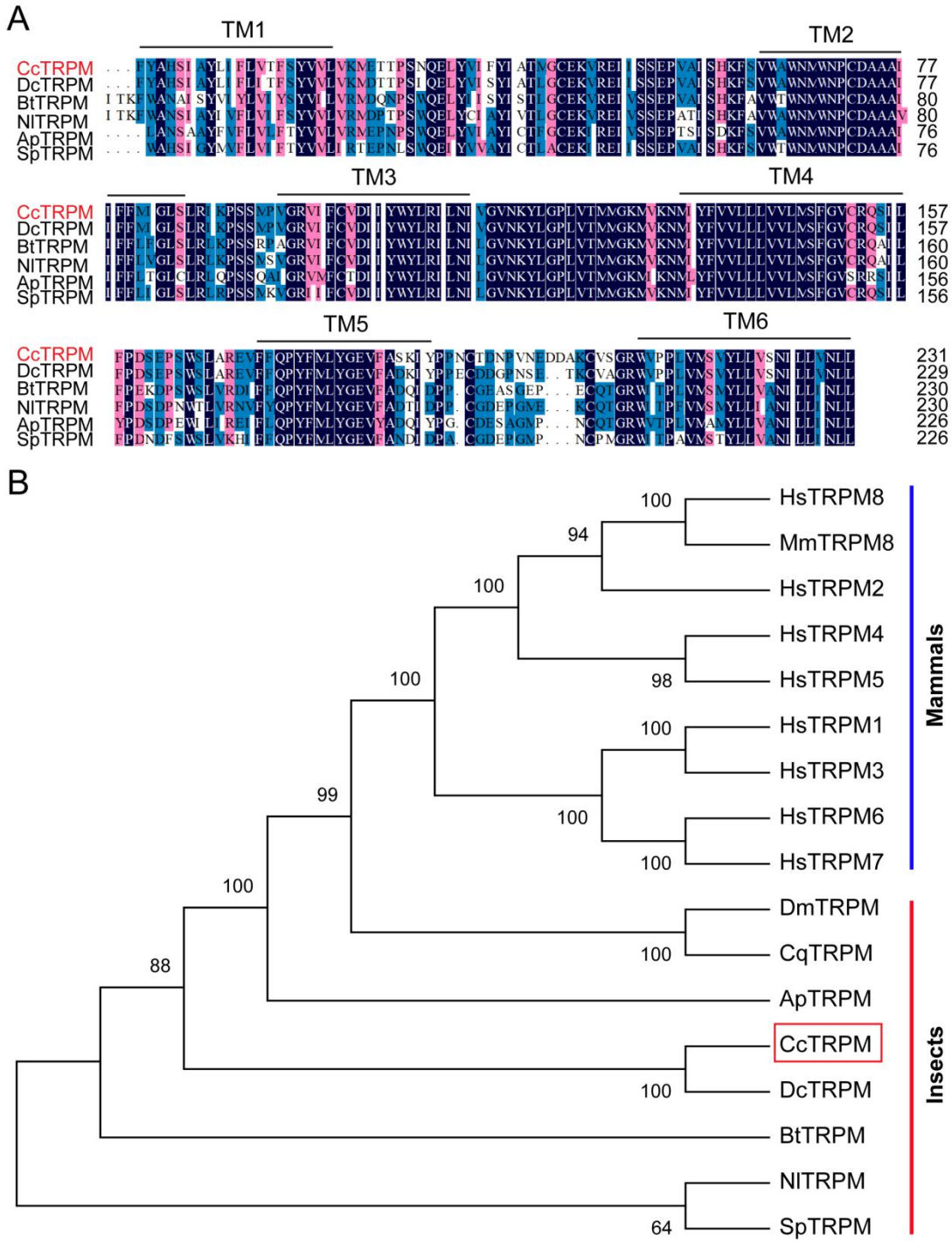

Figure S1. Sequence characterization of TRPM from different insect species.

A: Multiple alignments of the amino acid sequences of *CcTRPM* transmembrane domain with homologs from other insect species. Black represents 100% identity, red represents 75% identity and blue represents <75% identity. The transmembrane domain of TM1 to TM6 are indicated by black horizontal line. *CcTRPM* (*C. chinensis*, OQ658558), *DcTRPM* (*Diaphorina citri*, XP_017299512.2), *BtTRPM* (*Bemisia tabaci*, XP_018904971.1), *NlTRPM* (*Nilaparvata lugens*,

AOR81476.1), *ApTRPM* (*Acyrthosiphon pisum*, XP_003245193.1), *SpTRPM* (*Schistocerca piceifrons*, XP_047116036.1). The same as below.

B: Phylogenetic tree analysis of *CcTRPM* and its homologs in other insect species. *HsTRPM1* (*Homo sapiens*, NP_001238949.1), *HsTRPM2* (*Homo sapiens*, NP_001307279.2), *HsTRPM3* (*Homo sapiens*, NP_001353070.1), *HsTRPM4* (*Homo sapiens*, NP_060106.2), *HsTRPM5* (*Homo sapiens*, NP_055370.1), *HsTRPM6* (*Homo sapiens*, NP_060132.3), *HsTRPM7* (*Homo sapiens*, NP_060142.3), *HsTRPM8* (*Homo sapiens*, NP_001384540.1), *MmTRPM8* (*Mus musculus*, AAL79553.1), *DmTRPM* (*Drosophila melanogaster*, NP_001401007.1), *CqTRPM* (*Culex quinquefasciatus*, XP_038115236.1).

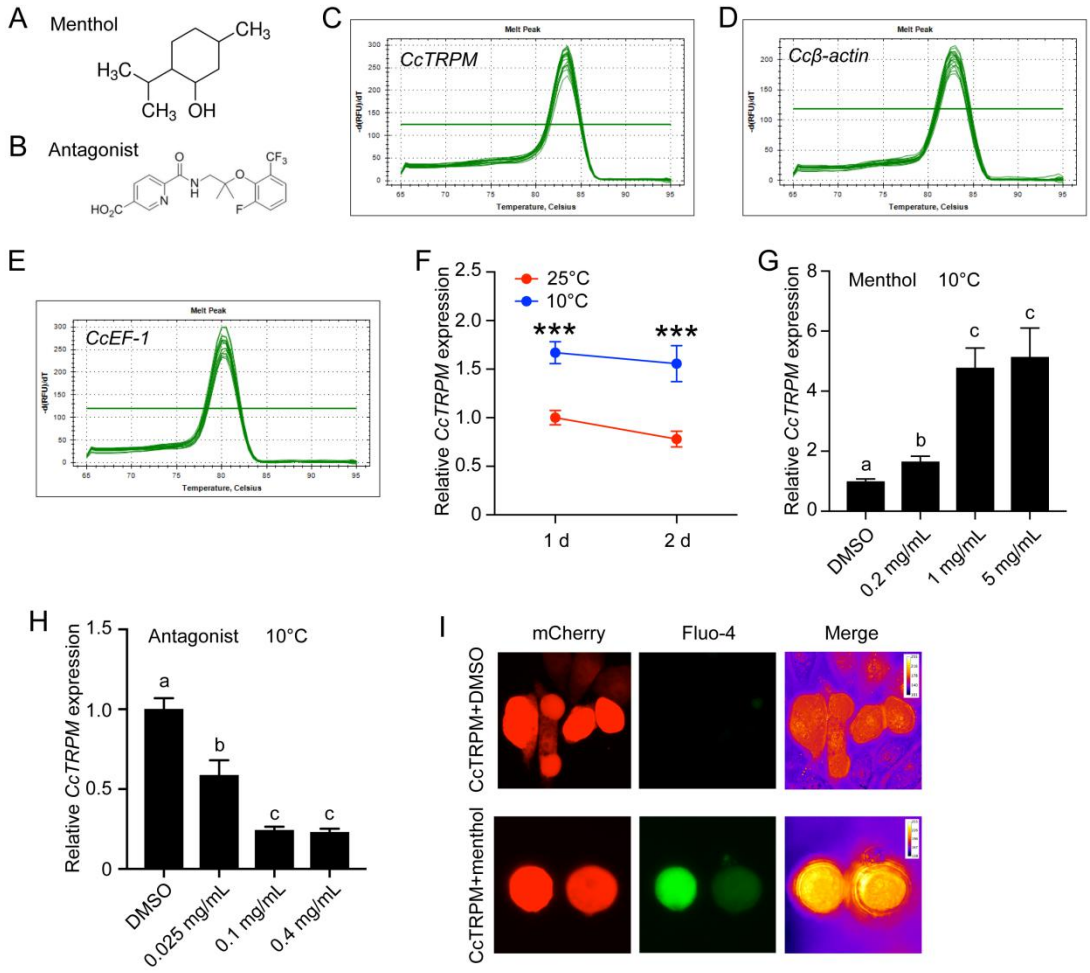

Figure S2. Effect of menthol and *CcTRPM* antagonist treatment on the mRNA expression of *CcTRPM* under 10 °C condition.

A-B: The chemical structure of menthol and TRPM antagonist.

C-E: Melting curve for qRT-PCR primers of *CcTRPM*, *Ccβ-actin* and *CcEF-1*.

F: The mRNA expression of *CcTRPM* in response to different temperatures of 25°C and 10°C at 1 d and 2 d by qRT-PCR.

G: Effect of menthol treatment at different concentrations on the mRNA expression of *CcTRPM* under 10 °C condition.

1063 H: Effect of TRPM antagonist treatment at different concentrations on the mRNA expression of
1064 *CcTRPM* under 10 °C condition.
1065 I: Representative images of Ca^{2+} imaging after heterologous expression of *CcTRPM* in
1066 mammalian HEK293T cells in response to menthol treatment. "CcTRPM+menthol" means the
1067 recombinant plasmid of *CcTRPM* with pcDNA3.1(+)-mCherry was treated with menthol.
1068 "CcTRPM+DMSO" denotes the pcDNA3.1(+)-mCherry plasmid with *CcTRPM* was treated with
1069 DMSO. mCherry and Fluo-4 signal are shown in red and green, respectively.
1070 Data are shown as mean ± SD with three biological replications. Different letters above the bars
1071 indicated statistically significant differences ($p < 0.05$), as determined by ANOVA followed with
1072 a Turkey's HSD multiple comparison test in SPSS 20.0 software.
1073
1074

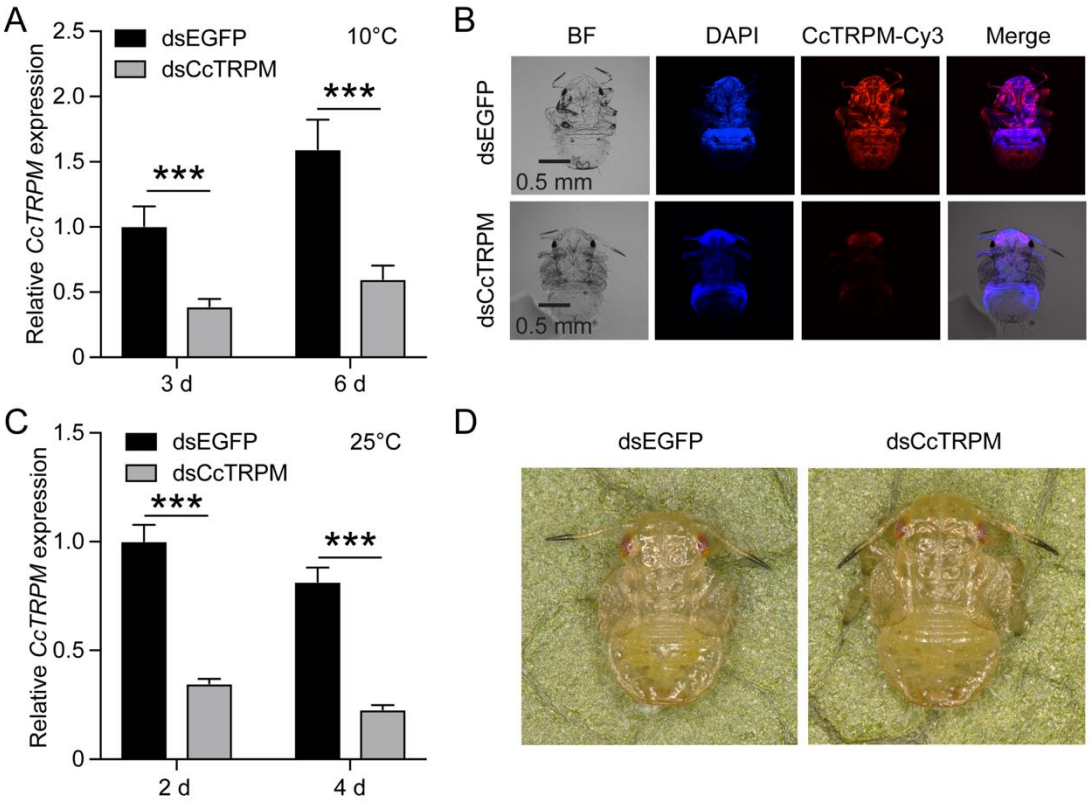

1075
1076 **Figure S3. RNAi efficiency of *CcTRPM* and effect of *CcTRPM* knockdown on the phenotype**
1077 **at 25 °C.**
1078 A: RNAi efficiency of *CcTRPM* after dsCcTRPM treatment at 3 d and 6 d by qRT-PCR under
1079 10 °C condition.
1080 B: Representative confocal images of *CcTRPM* after SF 1st instar nymphs treated with
1081 dsCcTRPM for 6 d at 10 °C by FISH. Scale bar is 0.5 mm. BF: the bright field. DAPI: the cell
1082 nuclei were stained with DAPI and visualized in blue. CcTRPM-Cy3: CcTRPM signal was
1083 labeled with Cy3 and visualized in red. Merge: merged imaging of BF, DAPI, and CcTRPM-Cy3
1084 signals.
1085 C: RNAi efficiency of *CcTRPM* after dsCcTRPM treatment at 2 d and 4 d by qRT-PCR under
1086 25 °C condition.
1087 D: The phenotype of SF 1st instar nymphs treated with dsEGFP and dsCcTRPM at 10 d under

25 °C condition.

Data are shown as mean ± SD with three biological replications. Statistically significant differences were determined with the pair-wise Student's *t*-test, and significance levels were denoted by *** ($p < 0.001$).

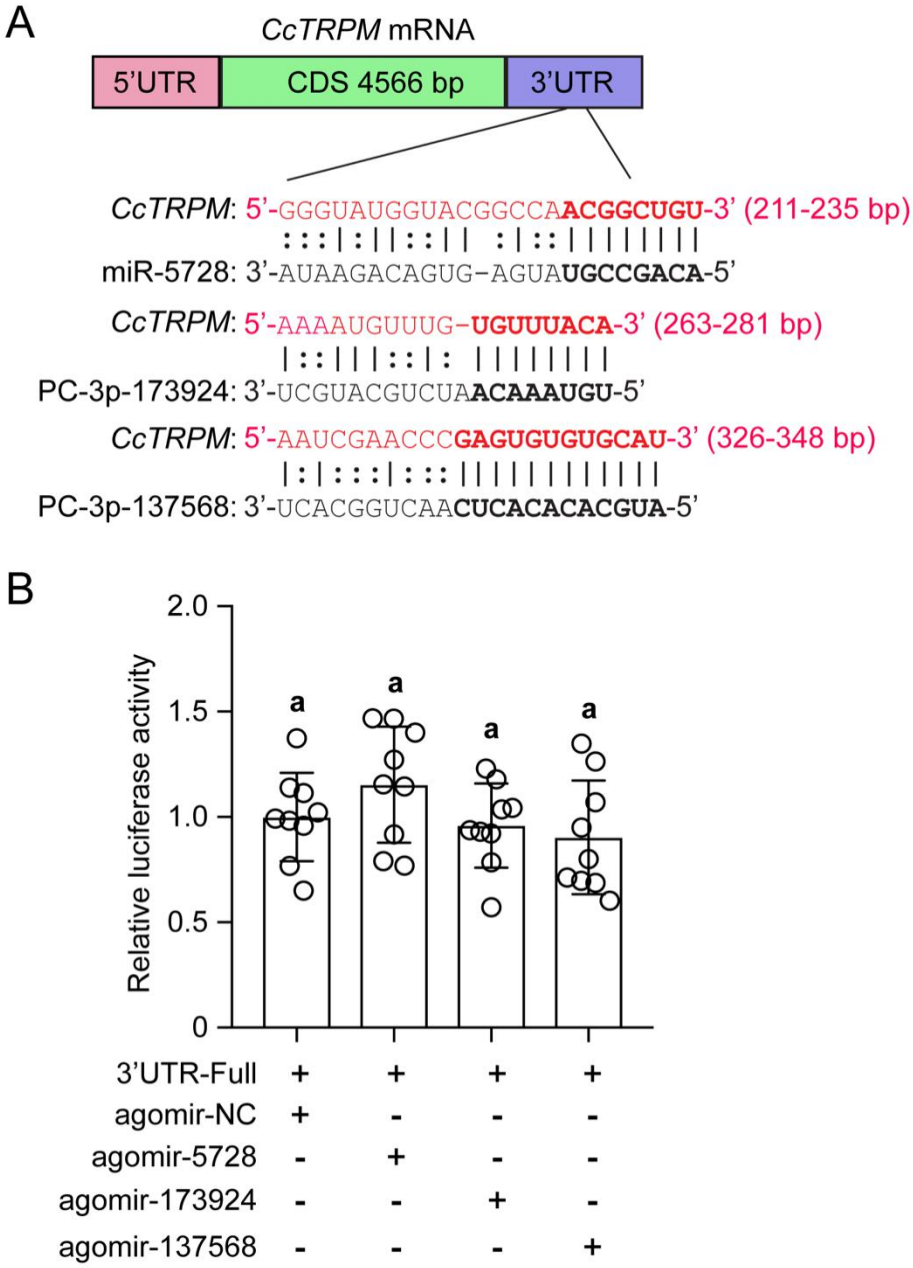

Figure S4. Validation of the target interactions between *CcTRPM* and other three miRNAs.

A: The putative binding sites of miR-5728, PC-3p-173924, and PC-3p-137568 in *CcTRPM* 3'UTR were predicted by miRanda and Targetscan.

B: In vitro validation of the target interactions between miR-5728, PC-3p-173924, and PC-3p-137568 with *CcTRPM* by dual luciferase reporter assays. Data are presented as mean ± SD with nine biological replications. Different letters above the bars indicated statistically significant differences ($p < 0.05$), as determined by ANOVA followed with a Turkey's HSD multiple

comparison test in SPSS 20.0 software.

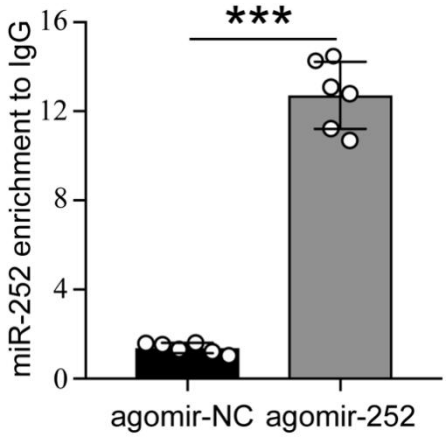

Figure S5. Transcript of miR-252 was significantly enriched by antibody against Ago1 in agomir-252 treated group compared with agomir-NC group.

Data are shown as mean ± SD with two biological replications of three technical replicates for each biological replication. Statistically significant differences were determined with the pair-wise Student's *t*-test, and significance levels were denoted by *** ($p < 0.001$).

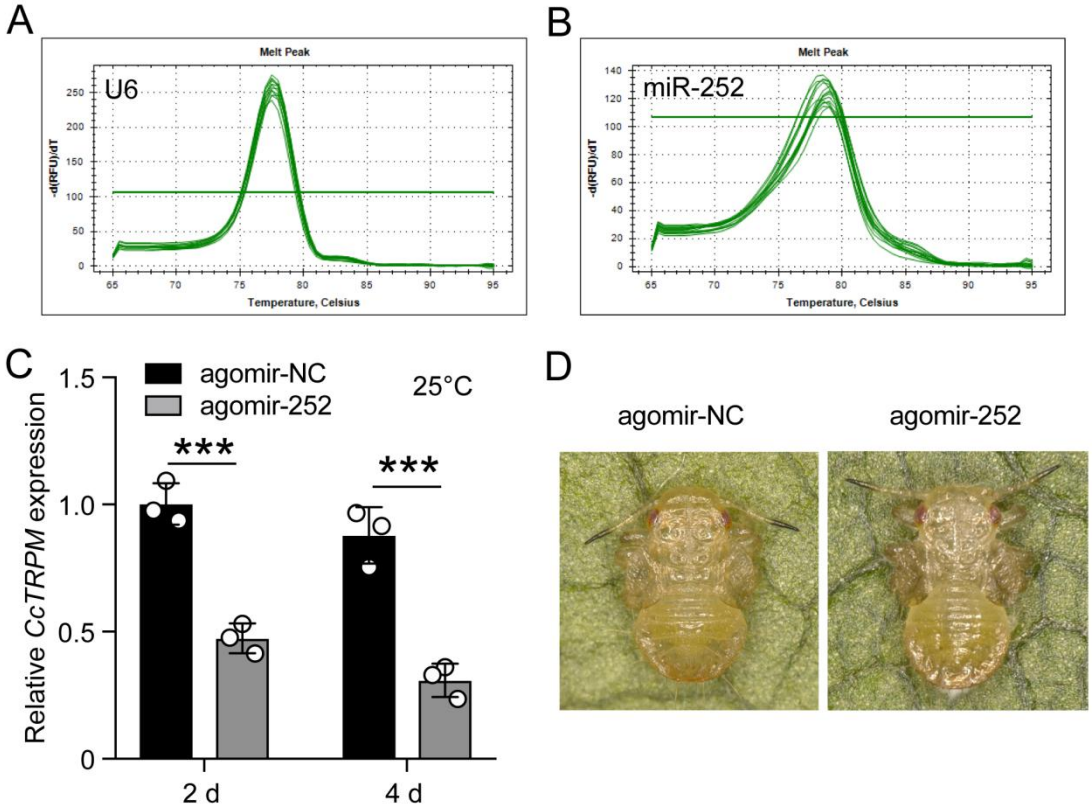

Figure S6. Effect of agomir-252 on the phenotype of SF 1st instar nymphs at 25 °C.

A-B: Melting curve for qRT-PCR primers of U6 and miR-252.

C: Effect of agomir-252 treatment 2 d and 4 d on the mRNA expression of *CcTRPM* under 25 °C condition.

D: The phenotype of SF 1st instar nymphs treated with agomir-NC and agomir-252 at 10 d at 25 °C.

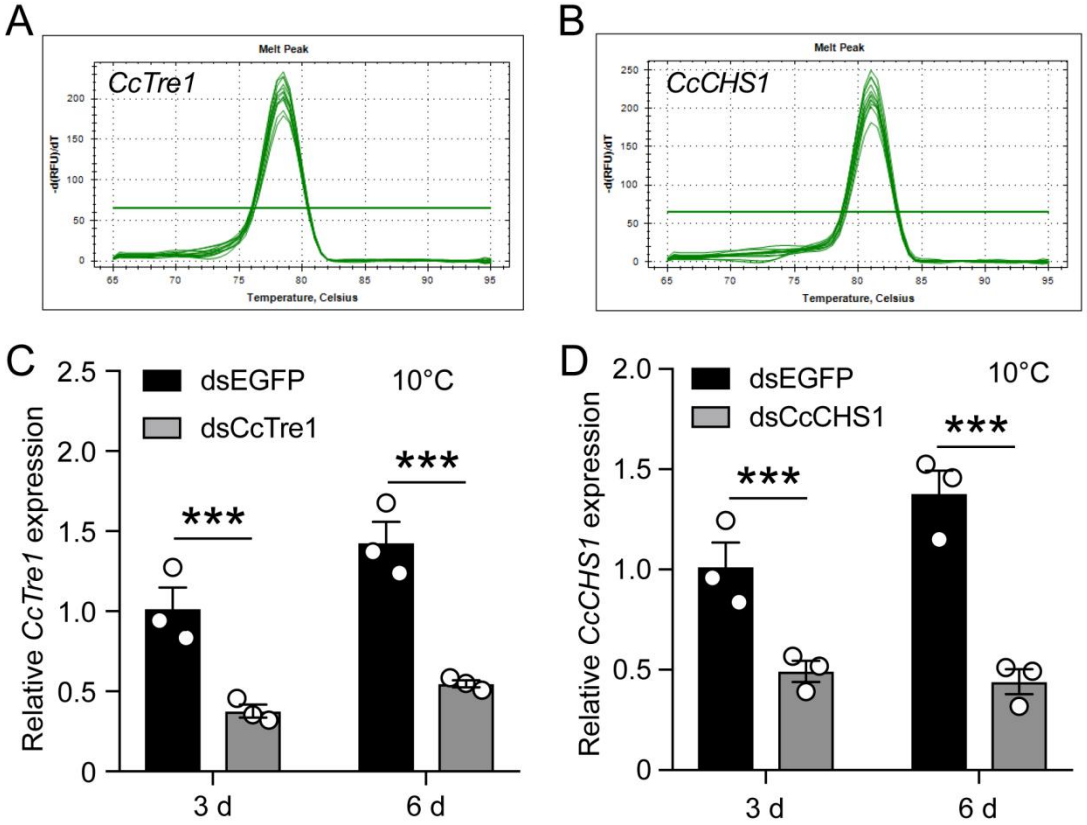

Figure S7. RNAi efficiency of *CcTre1* and *CcCHS1* at 10 °C by qRT-PCR.

A-B: Melting curve for qRT-PCR primers of *CcTre1* and *CcCHS1*.

C-D: RNAi efficiency of *CcTre1* and *CcCHS1* after dsCcTre1 and dsCcCHS1 treatment at 3 d and 6 d under 10 °C condition by qRT-PCR, respectively.

Data are shown as mean ± SD with three biological replications. Statistically significant differences were determined with the pair-wise Student's *t*-test, and significance levels were denoted by *** ($p < 0.001$).

1125 **Table S1. The primers used in current study.**

1126

Gene name (Abbreviation)	Accession number	Sequences (5'-3')	Production length (bp)	Purpose	Amplification efficiency
CcTRPM	OQ658558	Full-F1: GGATAGAGGCAACTTTTCAA Full-R1: ATCTATTCTGTCGTGCTCCA	1307	RT-PCR for sequence validation	—
		Full-F2: TAGACGAAGCCATGATGC Full-R2: ACAACTGTTTCACGGAGTGT	1162	RT-PCR for sequence validation	—
		Full-F3: TAGCCAGACATTCTCAACAA Full-R3: GAAGCATTACTATGGGTTGC	1436	RT-PCR for sequence validation	—
		Full-F4: AGCAGACCCTTTCCACTC Full-R4: TAACTGTTAACACATTGTTTCTGC	1334	RT-PCR for sequence validation	—
		qF: ACAATGCATTCTTCTTGACC qR: GACTTTGTACACTGGGGGTA	141	qRT-PCR	102.57
		RNAi-F1: GATCACTAATACGACTCACTATAGGGAGA GGTACCTTCGTATCCTCAAC RNAi-R1: GATCACTAATACGACTCACTATAGGGAGA TGGCATTGATCTCCATGAAA	472	dsRNA synthesis	—

		Probe: Cy3-CATAGATCGCGTAGGAGGTC	20	FISH	—
		3’UTR-Full-F1: CTAGTTGTTTAAACGAGCTC CATTATGTAACCACAGCGTAA 3’UTR-Full-R1: TGCATGCCTGCAGGTCGACTCTAGA TTCCTAGAAACTCAAAAATCG	419	Amplification of 3’UTR full sequence	—
		3’UTR-Mut-F1: CTAGTTGTTTAAACGAGCTC CATTATGTAACCACAGCGTAA 3’UTR-Mut-R1: TGCATGCCTGCAGGTCGACTCTAGA AAGTACTATCCACGCTCGAC	137	Amplification of 3’UTR mutant sequence	—
		Orf-F: GGACGAGCTGTACAAGTAGGGATCC ATGGAGAGGTCCCAGAGGTC Orf-R: GTTTAAACGGGCCCTCTAGACTCGAGC TTAACACATTGTTTCTGCGC	4618	Amplification of orf sequence	—
miR-252	-	qF: GCTAAGTACTGGTGCCGCAGGA	—	qRT-PCR	—
U6	-	qF: AGGATGACACGCAAAATCGT	—	qRT-PCR	—
CcTre1	OQ734934	qF: GGAACTCCCTCCTCTATGTT qR: CCAATAGTCAGCCAATCTGT	147	qRT-PCR	97.73

		RNAi-F1: GATCACTAATACGACTCACTATAGGGAGA AGATGTCAAAACCAATCCAG RNAi-R1: GATCACTAATACGACTCACTATAGGGAGA GGCCAAGTTGTAGTATTTGC	455	dsRNA synthesis	—
CcTre2	OQ734935	qF: CCAATCCTTCTCTACACCTG qR: CTGTCATTGTTGTACGGTTG	123	qRT-PCR	93.68
CcTre-like	OQ734936	qF: GACCGAACCTATGATCTCAA qR: AGATGTACCAAGCTGCTGAG	135	qRT-PCR	106.13
CcCHS1	OQ658570	F: AGAAGAGAAGAAACAGCAGG R: TAGTGTCCAATCGTTTCTCC	233	qRT-PCR	101.47
		RNAi-F1: GATCACTAATACGACTCACTATAGGGAGA TTGGCTACCACTGAGAAACT RNAi-R1: GATCACTAATACGACTCACTATAGGGAGA ATGCGTTTCGTACTCGTAAT	367	dsRNA synthesis	—
CcCHS2	OQ658569	F: TATTAGGCTGATGTTGCTGA R: GAGGCAACACAAGAGGTAAG	124	qRT-PCR	95.49
CcHK1	OQ658562	F: GAGTCTGCCATCTACTGTCC	130	qRT-PCR	96.21

		R: CGGGGGTGATATTTGTATAG			
CcHK2	OQ658560	F: AAATAGTCCGACTGGCATTA R: TGTACTCTTGGGCTCACTTT	137	qRT-PCR	98.05
CcHK3	OQ658561	F: AGCATTTGAGAGAGAACGTG R: CCGCTGATATTGTCTTCTTC	120	qRT-PCR	103.51
CcG6PI	OQ658563	F: CCTGCTATCTCTCACAATCC R: CTTTCAGTTCAGCTTCTGCT	127	qRT-PCR	107.23
CcGFAT	OQ658564	F: ACTGAAACATGGACCTCTTG R: CTTCCATCTCTGGCAATAAC	123	qRT-PCR	97.06
CcGNA	OQ658565	F: GGCGAGTATTTTGTGAGTGT R: CTCGGTACGTATCATCGACT	145	qRT-PCR	108.46
CcAGM	OQ658566	F: TTTATTTTGAGGCAAATGGT R: AAGAGTCTCCGACAGTTTCA	138	qRT-PCR	102.84
CcUAP1	OQ658567	F: TGGGGAACTTGTGTATAACC R: TGGAATCTTCTTGAGTGCTT	124	qRT-PCR	98.03
CcUAP2	OQ658568	F: ACATTGACTCCAAAGGATTG R: GGCAAAATCATGTTCTCTGT	134	qRT-PCR	89.74

CcEF-1	OQ658572	qF: TGTGTCGAGTCATTCTCTGA qR: TTACTTTACCGGAGGACAGA	124	Reference gene for qRT-PCR	98.63
Ccβ-Actin	OQ658571	qF: CAGCACCATGAAGATCAAG qR: GACTCGTCATACTCCTGCTT	129	Reference gene for qRT-PCR	102.87
EGFP	ACY56286	F: GATCACTAATACGACTCACTATAGGGAGA CTCCAGCAGGACCATGTGATC R: GATCACTAATACGACTCACTATAGGGAGA CCTGAAGTTCATCTGCACCAC	596	dsRNA synthesis	—

Note: The black boxes indicated the T7 promoter sequences in the primers of dsRNA synthesis. The underlines showed the homologous arm sequences for the seamless cloning in homologous recombination.

1131 **Table S2. Effect of agomir-252 and antagomir-252 treatment on the transition percent of SF 1st instar nymphs under 10°C.**

1132

Treatments	agomir-NC	agomir-252	dsEGFP	dsCcTRPM	dsCcTRPM+antagomir-252
Average percent	84.11 ± 8.37	38.89 ± 9.03	87.00 ± 5.79	31.56 ± 6.58	76.00 ± 7.78

1133

1134